

Which Coherence Decoheres?

Basis-Dependent Decoherence Rates in Symmetry-Broken Collective Spin Systems

Stavros Mouslopoulos

*Faculty of Science and Engineering, University of Nottingham Ningbo China
Ningbo 315100, China*

Stavros.Mouslopoulos@nottingham.edu.cn

Abstract

For a collective spin system in a symmetry-broken phase, there exist two natural bases: the localised states $\{|P\rangle, |R\rangle\}$ that maximise the order parameter within the low-energy doublet, and the energy eigenstates $\{|E_0\rangle, |E_1\rangle\}$ that diagonalise the Hamiltonian. Both bases yield well-controlled Lindblad dephasing rates for their respective coherences, and in the mesoscopic quantum regime, those rates differ. The exact diagonal Redfield coefficient for ρ_{PR} is $\gamma_\phi(G_{01} + J_{01}^2)$; the mean-field (spin-coherent) approximation gives the larger rate $\gamma_\phi G_{\text{loc}}$ where $G_{\text{loc}} = (Nm_*)^2/2$, which governs the pure exponential decay of $\text{Re}(\rho_{PR})$. The energy-eigenstate coherence ρ_{01} decays at rate $\gamma_\phi G_{01}$ where $G_{01} = \frac{1}{2}(\langle E_0 | \hat{J}_z^2 | E_0 \rangle + \langle E_1 | \hat{J}_z^2 | E_1 \rangle)$. These two questions yield different answers in two distinct senses: the *geometric* ratio $\eta_{\text{MF}} = G_{\text{loc}}/G_{01}$ approaches exactly 2 as $N \rightarrow \infty$ (a model-independent statement about matrix elements, valid even where the secular approximation fails); and at *finite* N in the LMG model, η_{MF} rises to a peak $\eta_{\text{MF}} \approx 2.42$ within the mesoscopic secular window ($2\Delta E \cdot T_2 \gg 1$, setting $\hbar = 1$), where both rates are simultaneously well-defined as exponential decay constants. The discrepancy in physical decay rates is therefore strictly a mesoscopic finite- N effect; the universal $\eta_{\text{MF}} = 2$ is a geometric statement that survives the breakdown of the secular approximation in the thermodynamic limit. In the thermodynamic limit ($N \rightarrow \infty$), the secular approximation fails, the doublet becomes degenerate, and the *decaying components* of both coherences converge exactly to the classical macroscopic (pointer-basis) rate $\gamma_\phi G_{\text{loc}}$, while $\text{Re}(\rho_{01})$ approaches a quasi-steady state (metastable plateau) within the doublet. At finite N , however, the secular approximation remains valid, and the two coherences decay at genuinely different rates. For quantum technologies — spin squeezing, quantum Fisher information, Leggett-Garg tests — this provides a quantitative quantum advantage *conditional on the protocol being sensitive to the eigenstate coherence ρ_{01} and remaining within the ground-state doublet*. Two distinct protection factors are relevant: $\eta_{\text{MF}} = G_{\text{loc}}/G_{01} \approx 2.42$ (peak), which quantifies the advantage over the classical mean-field pointer-state estimate $\gamma_\phi G_{\text{loc}}$; and $\eta_{\text{exact}} = (G_{01} + J_{01}^2)/G_{01} \approx 1.86$, which is the true basis-dependent physical protection factor — the exact ratio of the pointer-state decay rate $\gamma_\phi(G_{01} + J_{01}^2)$ to the eigenstate rate $\gamma_\phi G_{01}$. We demonstrate this protected three-regime structure in the Lipkin-Meshkov-Glick model via exact diagonalisation and provide the precise algebraic origin of the discrepancy via the \mathbb{Z}_2 parity of the Lindblad operator.

1 Introduction

The decoherence rate of a collective spin system is not a single number. It is a basis-dependent statement about which coherence is decaying, and at what rate.

This observation has a concrete consequence. In the ordered phase of any \mathbb{Z}_2 -symmetric collective spin model, two Lindblad-based calculations yield rates that differ by a factor approaching 2 as $N \rightarrow \infty$ and reaching 2.35–2.42 near the quantum-critical crossover at finite N . Neither calculation is wrong. They answer different questions. The localised-state calculation correctly describes the dephasing of $\rho_{PR} = \langle P|\rho|R\rangle$, the coherence between the exact symmetry-broken pointer states. The eigenstate calculation correctly describes the dephasing of $\rho_{01} = \langle E_0|\rho|E_1\rangle$, the coherence between energy eigenstates.

These are not the same object (see Eq. (8) for their relation); they decay at *different* rates in the mesoscopic secular window (e.g., $N \approx 250$ –430) where the secular approximation remains robust ($2\Delta E \cdot T_2 \gg 1$) and both rates are simultaneously well-defined. At finite N the discrepancy is amplified by near-critical wavefunction delocalisation.

This discrepancy is strictly a mesoscopic quantum phenomenon. In the macroscopic classical limit ($N \rightarrow \infty$), the secular approximation breaks down, the ground doublet becomes degenerate, and the exact Lindblad dynamics force the decaying components in *both* bases to converge to the fast rate $\gamma_\phi G_{\text{loc}}$, while $\text{Re}(\rho_{01})$ approaches a quasi-steady state (metastable plateau) within the doublet. The two pictures are not in contradiction; rather, the convergence of the physical rates marks the emergence of classical order-parameter relaxation (Section 3.3).

The rate difference exists solely in the finite- N regime, where quantum tunnelling ($\Delta E > 0$) dynamically protects the eigenstate coherence. For protocols sensitive to the eigenstate coherence ρ_{01} and operating effectively within the ground-state doublet, the relevant decoherence rate is therefore $\gamma_\phi G_{01}$ rather than the localised-state estimate $\gamma_\phi G_{\text{loc}}$, with quantum-coherence lifetimes longer by a factor of $\eta_{\text{exact}} \approx 1.86$ at $N = 370$ (the true physical basis-dependent protection), or up to $\eta_{\text{MF}} \approx 2.42$ when comparing against the classical mean-field pointer-state estimate. Note that this dynamically protected secular window ($N \approx 250$ –430) is broader than, and fully encompasses, the thermal “Goldilocks” zone ($N \approx 250$ –370) defined in the companion paper [1], where the additional constraint $\Delta E \gtrsim k_B T$ is required to suppress thermal noise in experimental implementations.¹

Relation to prior work. The basis dependence of decoherence is rooted in Zurek’s einselection programme [2], which identifies the pointer basis as the set of states stable under system-bath coupling. The Parity Proposition of Section 6 is conceptually adjacent to the decoherence-free-subspace construction [3], where a discrete symmetry of the system-bath coupling protects coherences within a symmetry sector; the present mechanism differs in that the eigenstate coherence ρ_{01} is not strictly protected but rather decays at a slower rate than the localised-state coherence by the universal factor $\eta_{\text{MF}} \rightarrow 2$. Dissipative dynamics in the LMG and Dicke models, including pointer-state selection by collective operators, symmetry-protected decoherence, and decoherence signatures of excited-state quantum phase transitions, have been studied extensively [4–7]. The factor-of- η_{MF} distinction analysed here is, to our knowledge, not previously isolated as a basis-dependent statement about two *simultaneously well-defined* dephasing rates in the mesoscopic secular window:

¹The temperature is set by $\Delta E(N = 370) = k_B T$, giving $T \approx 10$ nK for BEC-relevant parameters [1]. The thermal Goldilocks zone $\Delta E \gtrsim k_B T$ corresponds to $N \lesssim 370$; combining this with the secular condition $2\Delta E \cdot T_2 \gg 1$ (satisfied for $N \gtrsim 250$) defines the window $N \approx 250$ –370 where both thermal stability and quantum coherence are simultaneously optimised.

prior work has typically focused on the order-parameter rate $\gamma_\phi G_{\text{loc}}$ for symmetry-broken phases [8] or on the eigenstate rate $\gamma_\phi G_{01}$ for spectroscopic protocols [9, 11] but has not unified the two within a single framework with the explicit parity-based proposition we provide in Section 6.

The physical question is which coherence governs the observable of interest. For classical order-parameter relaxation, the localised basis is natural. For quantum-information protocols — spin squeezing [9, 10], quantum Fisher information [11], Leggett-Garg inequality tests [12, 13] — the relevant coherence is ρ_{01} , and the slower eigenstate rate is correct. Two distinct protection factors are relevant in this paper:

$$\eta_{\text{MF}}(N, \Gamma/J) \equiv \frac{G_{\text{loc}}}{G_{01}} = \frac{(Nm_*)^2/2}{\frac{1}{2}(\langle E_0 | \hat{J}_z^2 | E_0 \rangle + \langle E_1 | \hat{J}_z^2 | E_1 \rangle)}, \quad (1)$$

$$\eta_{\text{exact}}(N, \Gamma/J) \equiv \frac{G_{01} + J_{01}^2}{G_{01}} = 1 + \frac{J_{01}^2}{G_{01}}. \quad (2)$$

η_{MF} is the ratio of the classical mean-field pointer-state rate $\gamma_\phi G_{\text{loc}}$ to the exact eigenstate rate $\gamma_\phi G_{01}$; it approaches 2 as $N \rightarrow \infty$ and peaks at 2.42 near the crossover of the LMG model. η_{exact} is the ratio of the *exact* pointer-state decay rate $\gamma_\phi(G_{01} + J_{01}^2)$ to the eigenstate rate; at $N = 370$ it equals ≈ 1.86 . η_{MF} decomposes exactly as $\eta_{\text{MF}} = \eta_{\text{geom}} \times \eta_{\text{quantum}}$ (Section 3.1), where $\eta_{\text{geom}} = 2$ is a universal geometric factor from parity and $\eta_{\text{quantum}} > 1$ is a many-body Bogoliubov enhancement reaching 1.20 at the peak. The thermodynamic *geometric* limit $\eta_{\text{MF}} \rightarrow 2$ is universal for any collective spin system satisfying two conditions: (i) an isolated ground-state doublet arising from spontaneous \mathbb{Z}_2 symmetry breaking (so that the eigenstate expansion Eqs. (4)–(5) holds); (ii) a parity-odd Lindblad operator ($\hat{P}\hat{L}\hat{P}^\dagger = -\hat{L}$, as in Section 6). These two conditions are sufficient for the *geometric* ratio $G_{\text{loc}}/G_{01} \rightarrow 2$; the third condition — the secular approximation $2\Delta E \cdot T_2 \gg 1$ — is required for $\gamma_\phi G_{01}$ to be a physically meaningful exponential rate, but is not needed for the geometric statement. The specific peak value $\eta_{\text{MF}} \approx 2.42$ is LMG-specific, determined by the instanton action S_{inst} and the wavefunction delocalisation near the quantum-critical crossover.

The paper is organised as follows. Section 2 defines the two bases and coherences. Section 3 derives both dephasing rates, including the thermodynamic limit (Section 3.3) and the degenerate-doublet Lindblad treatment with the three-regime structure (Section 3.4). Section 4 addresses finite- N amplification. Section 5 presents the LMG model numerics. Section 6 gives the parity proposition. Section 7 discusses implications.

Table 1. Glossary of Key Notation. Summary of the primary physical parameters, geometric factors, and ratios used throughout this work.

Symbol	Definition
N, Γ, J	Number of spins, transverse field, and ferromagnetic coupling
m_*	Mean-field order parameter, $\sqrt{1 - \Gamma^2/J^2}$
ΔE	Quantum tunnel splitting between $ E_0\rangle$ and $ E_1\rangle$
γ_ϕ	Markovian collective dephasing rate
G_{loc}	Mean-field geometric factor, $(Nm_*)^2/2$
G_{01}	Exact eigenstate geometric factor, $\frac{1}{2}(\langle E_0 \hat{J}_z^2 E_0\rangle + \langle E_1 \hat{J}_z^2 E_1\rangle)$
J_{01}	Exact off-diagonal matrix element, $\langle E_0 \hat{J}_z E_1\rangle$
η_{MF}	Advantage over classical mean-field estimate, G_{loc}/G_{01}
η_{exact}	Exact basis-dependent physical protection factor, $(G_{01} + J_{01}^2)/G_{01}$

2 Two Bases, Two Coherences

Consider a collective spin- $\frac{1}{2}$ system of N particles with all-to-all ferromagnetic coupling $J > 0$ and transverse field Γ , described by the Kac-normalised Hamiltonian (the $1/N$ prefactor on the coupling ensures extensive energy in the thermodynamic limit [14])

$$\hat{H} = -\frac{2J}{N}\hat{J}_z^2 - 2\Gamma\hat{J}_x, \quad (3)$$

where $\hat{J}_z = \frac{1}{2}\sum_i \hat{\sigma}_i^z$ and $\hat{J}_x = \frac{1}{2}\sum_i \hat{\sigma}_i^x$. In the ordered phase ($\Gamma < J$) the \mathbb{Z}_2 symmetry generated by $\hat{P} = e^{i\pi\hat{J}_x}$ is spontaneously broken: the mean-field ground state bifurcates into two degenerate localised instanton vacua $|\tilde{P}\rangle$ and $|\tilde{R}\rangle$ with $\langle \tilde{P}|\hat{J}_z|\tilde{P}\rangle = +Nm_*/2$ and $\langle \tilde{R}|\hat{J}_z|\tilde{R}\rangle = -Nm_*/2$, where $m_* = \sqrt{1 - \Gamma^2/J^2}$ is the order parameter.

For finite N , the true eigenstates of \hat{H} are²:

$$|E_0\rangle = \frac{|\tilde{P}\rangle + |\tilde{R}\rangle}{\sqrt{2(1+S)}} = \frac{|\tilde{P}\rangle + |\tilde{R}\rangle}{\sqrt{2}} + \mathcal{O}(S), \quad (4)$$

$$|E_1\rangle = \frac{|\tilde{P}\rangle - |\tilde{R}\rangle}{\sqrt{2(1-S)}} = \frac{|\tilde{P}\rangle - |\tilde{R}\rangle}{\sqrt{2}} + \mathcal{O}(S), \quad (5)$$

where $S_{\text{inst}} = \text{arctanh}(m_*) - m_*$ is the WKB instanton action [1] governing the exponentially small tunnel splitting $\Delta E = E_1 - E_0 = C_0 N^{1/2} e^{-NS_{\text{inst}}}$ (at $\Gamma/J = 0.95$: $S_{\text{inst}} = 0.010787$, giving $\Delta E \approx 1310$ rad/s at $N = 370$ from exact diagonalisation); and $S \equiv \langle \tilde{P}|\tilde{R}\rangle = (\Gamma/J)^N \approx 5.7 \times 10^{-9}$ is the instanton-vacuum overlap at the benchmark. These two small quantities are physically distinct: $e^{-NS_{\text{inst}}} \approx 0.018$ governs the energy splitting ΔE , while $S \approx 5.7 \times 10^{-9}$ governs the $\mathcal{O}(S)$ wavefunction correction in Eqs. (4)–(5); they differ by a factor $\approx 3 \times 10^6$. Their parity eigenvalues are $p_0 = +1$ (even) and $p_1 = -1$ (odd).

²Readers comparing this work with the companion paper [1] should note a necessary shift in state notation. In Ref. [1], $|P\rangle$ and $|R\rangle$ denote the non-orthogonal mean-field spin-coherent states. Because the central thesis of the present work relies on the precise algebraic distinction between exact finite- N states and mean-field approximations, we strictly reserve $|P\rangle$ and $|R\rangle$ for the exact orthogonal pointer states defined in the energy doublet, using $|\tilde{P}\rangle$ and $|\tilde{R}\rangle$ (or $|P_{\text{SCS}}\rangle$ and $|R_{\text{SCS}}\rangle$) for the classical spin-coherent states.

We define the exact orthogonal pointer states of the low-energy doublet as $|P\rangle = (|E_0\rangle + |E_1\rangle)/\sqrt{2}$ and $|R\rangle = (|E_0\rangle - |E_1\rangle)/\sqrt{2}$.

The system supports two distinct coherences:

$$\rho_{PR} \equiv \langle P|\rho|R\rangle \quad (\text{localised-state coherence}), \quad (6)$$

$$\rho_{01} \equiv \langle E_0|\rho|E_1\rangle \quad (\text{eigenstate coherence}). \quad (7)$$

They are generically distinct. Using the exact orthogonal pointer states, one finds the exact algebraic identity:

$$\rho_{01} = \frac{1}{2}(\rho_{PP} - \rho_{RR}) - \frac{1}{2}(\rho_{PR} - \rho_{RP}). \quad (8)$$

Under the additional conditions $\rho_{PP} = \rho_{RR}$ (equal localised populations) and ρ_{PR} purely imaginary ($\rho_{PR} = iy$, $\rho_{RP} = -iy$), one finds $\rho_{01} = -\rho_{PR}$: equal in magnitude but opposite in sign, differing by an overall relative phase of π that leaves the decay rates invariant but profoundly alters the physical observables of the coherence. All three conditions (well-developed double-well, equal populations, purely imaginary ρ_{PR}) are special cases; the coherences are generically distinct.

Table 2. Taxonomy of Quantum and Classical States. Summary of the five distinct state types discussed in this work, classified by their physical regime (Quantum, Semi-Classical, Classical). The instanton vacua $|\tilde{P}\rangle, |\tilde{R}\rangle$ are the WKB saddle-point states that mediate between the exact quantum pointer states and the classical mean-field product states; their overlap $S = \langle \tilde{P} | \tilde{R} \rangle = (\Gamma/J)^N$ governs the $\mathcal{O}(S)$ corrections in the eigenstate expansions. The distinction between the exact quantum pointer states and the classical mean-field SCS is the physical origin of the η_{exact} vs η_{MF} discrepancy.

State / Basis	Definition & Relation	Mesoscopic Regime ($N \approx 250\text{--}430$)	Thermodynamic Limit ($N \rightarrow \infty$)
Energy Eigenstates [EXACT QUANTUM] $\{ E_0\rangle, E_1\rangle\}$	Exact eigenstates of \hat{H} . Definite \mathbb{Z}_2 parity ($p_0 = +1, p_1 = -1$). $ E_{0,1}\rangle = \frac{1}{\sqrt{2}}(P\rangle \pm R\rangle)$.	Form a quasi-degenerate doublet ($\Delta E > 0$). Decay rate: $\gamma_\phi G_{01}$.	Exactly degenerate ($\Delta E \rightarrow 0$). Secular approx. fails.
Exact Pointer States [EXACT QUANTUM] $\{ P\rangle, R\rangle\}$	Bath-selected states; exact eigenstates of \hat{J}_z <i>within the doublet</i> . $ P, R\rangle = \frac{1}{\sqrt{2}}(E_0\rangle \pm E_1\rangle)$. $ P\rangle = \tilde{P}\rangle + \mathcal{O}(S)$.	Macroscopically distinct but spin-squeezed by Bogoliubov depletion: $\langle \hat{J}_z \rangle = J_{01} < Nm_*/2$. Redfield coefficient: $\gamma_\phi(G_{01} + J_{01}^2)$.	Converge to instanton vacua ($\mathcal{O}(S) \rightarrow 0$) and thence to classical mean-field states.
Instanton Vacua (WKB) [SEMI-CLASSICAL] $\{ \tilde{P}\rangle, \tilde{R}\rangle\}$	WKB saddle-point states; non-orthogonal ($\langle \tilde{P} \tilde{R} \rangle = S = (\Gamma/J)^N$). $\langle \tilde{P} \hat{J}_z \tilde{P} \rangle = +Nm_*/2$ exactly (This is the definition of the WKB saddle-point state's center.). Appear in eigenstate expansions: $ E_{0,1}\rangle = \frac{ \tilde{P}\rangle \pm \tilde{R}\rangle}{\sqrt{2}} + \mathcal{O}(S)$.	Approximate exact pointer states with correction $\mathcal{O}(S) \approx 5.7 \times 10^{-9}$. Differ from SCS states by Bogoliubov depletion $\Delta_{\text{zp}} \sim \mathcal{O}(1)$. Not eigenstates of \hat{H} .	$S \rightarrow 0$: become orthogonal and converge to exact pointer states. Still differ from SCS by $\mathcal{O}(N^{-1})$.
Mean-Field States (Spin-Coherent) [CLASSICAL] $\{ P_{\text{SCS}}\rangle, R_{\text{SCS}}\rangle\}$	Classical product states minimising the mean-field free energy. $\langle \hat{J}_z \rangle = \pm Nm_*/2$ exactly by construction. Differ from $ \tilde{P}\rangle$ by Bogoliubov corrections $\mathcal{O}(N^{-1})$.	Overestimate true pointer magnetisation by $\Delta_{\text{zp}} \sim \mathcal{O}(1)$, inflating the decay rate by $\approx 26\%$. Decay rate: $\gamma_\phi G_{\text{loc}}$.	Become the exact ground states of the system; corrections vanish.
Dicke States [MICROSCOPIC BASIS] $\{ J_t, m\rangle\}$	Exact eigenstates of \hat{J}^2 and \hat{J}_z with eigenvalues $J_t(J_t + 1)$ and m ($J_t = N/2$). Computational basis in which \hat{H} is tridiagonal.	Pointer states are localised wavepackets spanning many m -states around $\pm J_{01}$.	Form a continuous macroscopic variable $m_z = m/(N/2)$.

3 Two Dephasing Rates

Subject the system to Markovian collective dephasing with Lindblad operator $\hat{L} = \sqrt{\gamma_\phi} \hat{J}_z$:

$$\dot{\rho} = -i[\hat{H}, \rho] + \gamma_\phi \left(\hat{J}_z \rho \hat{J}_z - \frac{1}{2} \hat{J}_z^2 \rho - \frac{1}{2} \rho \hat{J}_z^2 \right). \quad (9)$$

We define two dimensionless geometric factors:

$$G_{\text{loc}} \equiv \frac{(Nm_*)^2}{2}, \quad (10)$$

$$G_{01} \equiv \frac{1}{2} \left(\langle E_0 | \hat{J}_z^2 | E_0 \rangle + \langle E_1 | \hat{J}_z^2 | E_1 \rangle \right). \quad (11)$$

The mean-field dephasing rate is $\gamma_\phi G_{\text{loc}}$; the exact eigenstate rate is $\gamma_\phi G_{01}$.

3.1 The unified dephasing rate formula

For any Hermitian Lindblad operator $\hat{L} = \sqrt{\gamma_\phi} \hat{J}_z$, the dephasing rate of the coherence $\rho_{AB} = \langle A | \rho | B \rangle$ between any two states $|A\rangle$ and $|B\rangle$ follows directly from projecting Eq. (9):

$$\Gamma_{AB} = \frac{\gamma_\phi}{2} \left[\langle A | \hat{J}_z^2 | A \rangle + \langle B | \hat{J}_z^2 | B \rangle - 2 \langle A | \hat{J}_z | A \rangle \langle B | \hat{J}_z | B \rangle \right]. \quad (12)$$

Equation (12) is the *exact diagonal Redfield coefficient* — the coefficient of ρ_{AB} in the full projected equation $\dot{\rho}_{AB} = -i\omega_{AB}\rho_{AB} - \Gamma_{AB}\rho_{AB} + (\text{off-diagonal couplings})$. It requires no approximation to compute; in particular, the $\langle A | \hat{J}_z^2 | A \rangle$ terms implicitly include all leakage to higher states via the completeness identity $\langle A | \hat{J}_z^2 | A \rangle = \sum_k |\langle A | \hat{J}_z | k \rangle|^2$ (Section 3.4, Eq. (25)). However, obtaining a *pure exponential decay* $\dot{\rho}_{AB} = -\Gamma_{AB}\rho_{AB}$ requires additional approximations to eliminate these off-diagonal couplings [15]. For the eigenstate coherence ρ_{01} , the secular approximation drops the $\gamma_\phi |J_{01}|^2$ coupling to ρ_{10} (Corollary 2, Section 6), while population-coherence decoupling is exact by parity (Corollary 1). For the localised coherence ρ_{PR} , a mean-field (SCS) approximation is used, which effectively closes the dynamics to the two-state pointer sector. Under this approximation, the two-channel structure detailed in Appendix B then reveals that only $\text{Re}(\rho_{PR})$ undergoes pure exponential decay at rate Γ_{PR} , while $\text{Im}(\rho_{PR})$ exhibits damped oscillations. Equation (12) is nevertheless the natural comparison formula: applied to both bases it reveals the geometric origin of the rate difference without requiring either approximation to be invoked, because the cross-term difference between the two bases is an exact algebraic fact.

Applying it to the two natural bases makes the origin of the rate difference immediately transparent:

Eigenstate basis $\{|E_0\rangle, |E_1\rangle\}$: By the Parity Proposition (Section 6), $\langle E_i | \hat{J}_z | E_i \rangle = 0$ exactly. The cross-term vanishes:

$$\Gamma_{01} = \frac{\gamma_\phi}{2} (\langle E_0 | \hat{J}_z^2 | E_0 \rangle + \langle E_1 | \hat{J}_z^2 | E_1 \rangle - 2 \cdot 0 \cdot 0) = \gamma_\phi G_{01}. \quad (13)$$

Localised basis $\{|P\rangle, |R\rangle\}$: Using $|P, R\rangle = (|E_0\rangle \pm |E_1\rangle)/\sqrt{2}$ and the parity proposition, the pointer states have $\langle P | \hat{J}_z | P \rangle = \frac{1}{2}(J_{01} + J_{01}^*) = \text{Re}(J_{01})$. Because the LMG Hamiltonian is a real symmetric matrix, its eigenstates are purely real, making J_{01} strictly real. Thus, $\langle P | \hat{J}_z | P \rangle = +J_{01}$ and similarly $\langle R | \hat{J}_z | R \rangle = -J_{01}$. The cross-term is $-2(+J_{01})(-J_{01}) = +2J_{01}^2 > 0$:

$$\Gamma_{PR} = \frac{\gamma_\phi}{2} (\langle P | \hat{J}_z^2 | P \rangle + \langle R | \hat{J}_z^2 | R \rangle + 2J_{01}^2) = \gamma_\phi (\langle P | \hat{J}_z^2 | P \rangle + J_{01}^2). \quad (14)$$

Physical origin of the rate difference

The entire difference between Γ_{PR} and Γ_{01} arises from the cross-term $-2\langle A|\hat{J}_z|A\rangle\langle B|\hat{J}_z|B\rangle$ in Eq. (12):

- In the *eigenstate* basis the cross-term is *exactly zero* by parity: $\langle E_i|\hat{J}_z|E_i\rangle = 0$.
- In the *localised* basis the cross-term is $+2J_{01}^2 \approx 2G_{01}$ (large and positive), roughly doubling the rate.

Since $\langle P|\hat{J}_z^2|P\rangle = \frac{1}{2}(\langle E_0|\hat{J}_z^2|E_0\rangle + \langle E_1|\hat{J}_z^2|E_1\rangle) = G_{01}$ (the cross-terms $\langle E_0|\hat{J}_z^2|E_1\rangle$ vanish exactly because \hat{J}_z^2 is parity-even), Eq. (14) gives $\Gamma_{PR} = \gamma_\phi(G_{01} + J_{01}^2) \approx 2\gamma_\phi G_{01}$ in the thermodynamic limit where $J_{01}^2 \rightarrow G_{01}$.

The remaining subsections derive the two rates from the full Lindblad equation and state the approximations involved.

Projecting Eq. (9) onto $\langle P|\cdot|R\rangle$, the dominant dissipative contribution is:

$$\dot{\rho}_{PR}|_{\text{diss}} \simeq -\frac{\gamma_\phi}{2}(\langle P|\hat{J}_z|P\rangle - \langle R|\hat{J}_z|R\rangle)^2 \rho_{PR} = -\gamma_\phi G_{\text{loc}} \rho_{PR}. \quad (15)$$

The \simeq reflects two distinct approximations, each introducing an $\mathcal{O}(N^{-1})$ relative error in the localised rate.

Approximation 1 — SCS mean: $|P\rangle$ is identified with the spin-coherent state $|P_{\text{SCS}}\rangle$, replacing the exact finite- N mean $J_{01} = \langle P|\hat{J}_z|P\rangle$ with the thermodynamic asymptote $Nm_*/2$. The exact pointer state $|P\rangle = (|E_0\rangle + |E_1\rangle)/\sqrt{2}$ is *not* a spin-coherent state: it is spin-squeezed by intra-well zero-point quantum fluctuations (Bogoliubov spin-wave depletion). As a result, $J_{01} < Nm_*/2$ with a shift of $\mathcal{O}(1)$ (numerically: $Nm_*/2 - J_{01} \approx 6-8$ for $N = 500-2000$), giving a relative error of $\mathcal{O}(1)/\mathcal{O}(N) = \mathcal{O}(N^{-1})$. This error is completely separate from, and much larger than, the $\mathcal{O}(S)$ overlap corrections in Eqs. (4)–(5), which describe the relation between energy eigenstates and the symmetry-broken pointer states $|P\rangle, |R\rangle$ — not between $|P\rangle$ and $|P_{\text{SCS}}\rangle$.

Approximation 2 — SCS variance: The spin-coherent-state second moment is approximated as:

$$\langle P_{\text{SCS}}|\hat{J}_z^2|P_{\text{SCS}}\rangle = \left(\frac{Nm_*}{2}\right)^2 + \frac{N(1-m_*^2)}{4} \simeq \left(\frac{Nm_*}{2}\right)^2,$$

dropping the $\mathcal{O}(N)$ spin-coherent-state variance $N(1-m_*^2)/4$, a relative error of $(1-m_*^2)/(Nm_*^2) = \mathcal{O}(N^{-1})$.

While both relative errors scale as $\mathcal{O}(N^{-1})$ and vanish in the thermodynamic limit, at the finite- N benchmark ($N = 370$, $\Gamma/J = 0.95$, $m_* = 0.312$) the Bogoliubov depletion dominates. The exact pointer rate factor is $G_{01} + J_{01}^2 \approx 5290.2$, whereas the mean-field approximation yields $G_{\text{loc}} \approx 6673.9$. The mean-field rate G_{loc} therefore overestimates the exact pointer rate by $(G_{\text{loc}} - (G_{01} + J_{01}^2))/(G_{01} + J_{01}^2) \approx 26.2\%$ (equivalently, the exact rate is 20.7% below G_{loc}). This substantial $\mathcal{O}(1)$ finite- N discrepancy highlights precisely why the macroscopic mean-field rate formula overestimates the exact quantum decoherence in the mesoscopic regime.

The dissipator additionally leaves the localised population difference $\Delta\rho \equiv \rho_{PP} - \rho_{RR}$ invariant at leading order in the SCS approximation: $|P\rangle$ and $|R\rangle$ are approximate eigenstates of \hat{J}_z at $\pm Nm_*/2$, hence approximate steady states of the dephasing dissipator

(see Appendix B, Eq. (43)). At finite N where $\Delta E > 0$, the Hamiltonian then couples the imaginary part of ρ_{PR} to $\Delta\rho$, splitting the dynamics into two channels. The real part $\text{Re}(\rho_{PR})$ decouples from this system and undergoes pure exponential decay at $\gamma_\phi G_{\text{loc}}$ (Eq. (15), which captures this channel). The imaginary part $\text{Im}(\rho_{PR})$ and the population difference $\Delta\rho \equiv \rho_{PP} - \rho_{RR}$ form a coupled 2-component system whose dynamics are governed by the characteristic polynomial $\lambda^2 + \gamma_\phi G_{\text{loc}}\lambda + \Delta E^2 = 0$ (derived explicitly in Appendix B). In the mesoscopic secular regime where $\Delta E \gg \gamma_\phi G_{\text{loc}}$, the discriminant is negative: $\text{Im}(\rho_{PR})$ and $\Delta\rho$ undergo *damped oscillations* at frequency ΔE with an envelope decaying at $\gamma_\phi G_{\text{loc}}/2$ [15]. This envelope rate equals $\gamma_\phi G_{01}$ only in the thermodynamic limit $\eta_{\text{MF}} \rightarrow 2$; at finite N it exceeds $\gamma_\phi G_{01}$ by the factor $\eta_{\text{MF}}/2$. For the purposes of this paper, only the real-part channel is relevant: it gives the pure exponential decay of the order-parameter coherence at the mean-field rate $\gamma_\phi G_{\text{loc}}$.

3.2 Rate for ρ_{01}

In the energy eigenstate basis, the secular Lindblad equation gives:

$$\dot{\rho}_{01}|_{\text{diss}} = -\gamma_\phi G_{01} \rho_{01}. \quad (16)$$

The secular approximation drops the off-diagonal term $\gamma_\phi |\langle E_0 | \hat{J}_z | E_1 \rangle|^2$ coupling ρ_{01} to ρ_{10} . In the interaction picture both counter-rotate at $\omega_{01} \equiv \Delta E/\hbar$ (the Bohr frequency of the ground doublet), so their coupling oscillates at $2\Delta E/\hbar$; the secular condition is thus $(2\Delta E/\hbar) \cdot T_2 \gg 1^3$, where $T_2 \equiv (\gamma_\phi G_{01})^{-1}$ is the eigenstate coherence decay time (formalised in Corollary 2, Section 6). At the LMG benchmark ($N = 370$, $\Gamma/J = 0.95$, $\gamma_\phi = 0.05 \text{ s}^{-1}$), $(2\Delta E/\hbar) \cdot T_2 \approx 18.4$ [1].

Crucially, the population-to-coherence coupling in the Redfield tensor vanishes exactly by parity for the ground doublet (Corollary 1, Section 6): ρ_{01} decouples from populations ρ_{00} , ρ_{11} without secular approximation. This decoupling is exact within the Markovian Lindblad dissipator of Eq. (9); it relies on the parity proposition $\langle E_i | \hat{J}_z | E_i \rangle = 0$ (all i) and $\langle E_j | \hat{J}_z^2 | E_i \rangle = 0$ for opposite-parity pairs (see Section 6).

The ratio of the two geometric factors, Eq. (1), equals the ratio of physical rates (the γ_ϕ cancels).

It is illuminating to decompose η_{MF} into two physically distinct factors:

$$\eta_{\text{MF}} = \eta_{\text{geom}} \times \eta_{\text{quantum}}, \quad (17)$$

where:

$$\eta_{\text{geom}} \equiv 2, \quad (18)$$

$$\eta_{\text{quantum}} \equiv \frac{(Nm_*/2)^2}{G_{01}} \geq 1. \quad (19)$$

$\eta_{\text{geom}} = 2$ is the *universal geometric factor*: it is the exact thermodynamic-limit value of η_{MF} , arising purely from the vanishing of the cross-term in the eigenstate basis (as shown in the keyresult above), and is independent of model parameters. $\eta_{\text{quantum}} \geq 1$ is the *many-body quantum enhancement*: it exceeds unity because Bogoliubov spin-wave depletion suppresses G_{01} below the mean-field reference $(Nm_*/2)^2$ (Section 3.4). The

³Here and throughout, we frequently set $\hbar = 1$ for brevity, such that the energy splitting ΔE corresponds directly to the coherent tunnelling angular frequency.

decomposition is exact: since $G_{\text{loc}} = (Nm_*)^2/2 = 2(Nm_*/2)^2$, we have $\eta_{\text{MF}} = G_{\text{loc}}/G_{01} = 2(Nm_*/2)^2/G_{01} = \eta_{\text{geom}} \times \eta_{\text{quantum}}$.

At the benchmark $N = 370$: $\eta_{\text{quantum}} = 1.175$, giving $\eta_{\text{MF}} = 2 \times 1.175 = 2.35$. At the peak $N \approx 300$: $\eta_{\text{quantum}} = 1.201$, giving $\eta_{\text{MF}} = 2 \times 1.201 = 2.40$. The full $\approx 21\%$ enhancement above the geometric baseline ($\eta_{\text{quantum}} - 1 \approx 0.2$) arises from many-body quantum fluctuations near the quantum-critical crossover and reflects the Bogoliubov suppression of G_{01} below the mean-field reference.

The *exact* physical protection factor is separately: $\eta_{\text{exact}} = (G_{01} + J_{01}^2)/G_{01} = 1 + J_{01}^2/G_{01}$. At $N = 370$: $\eta_{\text{exact}} = (2839 + 2451)/2839 = 1.863$. The difference $\eta_{\text{MF}}/\eta_{\text{exact}} = G_{\text{loc}}/(G_{01} + J_{01}^2) \approx 1.262$ reflects the 26.2% overestimation by the SCS mean-field approximation (Section 3, Approximations 1–2).

3.3 The thermodynamic limit and the factor of 2

Because the pointer states are defined exactly as $|P, R\rangle = (|E_0\rangle \pm |E_1\rangle)/\sqrt{2}$, and \hat{J}_z^2 is parity-even (making the cross-terms $\langle E_0|\hat{J}_z^2|E_1\rangle$ vanish exactly), the doublet average G_{01} corresponds precisely to the exact pointer-state second moment at any finite N :

$$G_{01} = \frac{1}{2}\langle P|\hat{J}_z^2|P\rangle + \frac{1}{2}\langle R|\hat{J}_z^2|R\rangle = \left(\frac{Nm_*}{2}\right)^2 - \delta G(N, \Gamma/J) + \mathcal{O}(1), \quad (20)$$

where $\delta G > 0$ is the quantum-delocalisation correction of Eq. (31): the exact eigenstate wavefunction spreads into the classically forbidden barrier region, suppressing G_{01} *below* the mean-field reference $(Nm_*/2)^2$. Note that Eq. (20) is an exact identity at each finite N ; the thermodynamic limit $G_{01} \rightarrow (Nm_*/2)^2$ is recovered simply because the finite- N quantum correction $\delta G \sim \mathcal{O}(N)$ becomes subleading to the $\mathcal{O}(N^2)$ mean-field baseline.

This should be contrasted with the mean-field spin-coherent state $|P_{\text{SCS}}\rangle$, defined as the product state (SCS) satisfying $\langle P_{\text{SCS}}|\hat{J}_z|P_{\text{SCS}}\rangle = +Nm_*/2$ exactly by construction. It is *not* identical to the exact pointer state $|P\rangle$ at finite N : the exact state is the half-sum of eigenstates $(|E_0\rangle + |E_1\rangle)/\sqrt{2}$, whose mean magnetisation satisfies $|\langle P|\hat{J}_z|P\rangle| = J_{01} \leq Nm_*/2$ (with the approach to $Nm_*/2$ controlled by the same exponentially small corrections as Eqs. (4)–(5)). The SCS second moment is:

$$\langle P_{\text{SCS}}|\hat{J}_z^2|P_{\text{SCS}}\rangle = \left(\frac{Nm_*}{2}\right)^2 + \frac{N(1 - m_*^2)}{4}. \quad (21)$$

The spin-coherent-state variance $N(1 - m_*^2)/4$ adds a *positive* $\mathcal{O}(N)$ correction — of *opposite* sign to the $-\delta G$ correction for the exact eigenstate. Both corrections are subleading at $\mathcal{O}(N^{-1})$ relative to $(Nm_*/2)^2$. The SCS approximation $|P\rangle \approx |P_{\text{SCS}}\rangle$ is used implicitly in the localised-state rate derivation of Section 3 (where $\langle P|\hat{J}_z|P\rangle$ is set to $+Nm_*/2$); this introduces a relative error of $\mathcal{O}(N^{-1})$ from Bogoliubov spin-wave depletion (distinct from, and much larger than, the $\mathcal{O}(S)$ vacuum overlap corrections in Eqs. (4)–(5), which describe the eigenstate-to-pointer-state relation, not the pointer-to-SCS relation).

In the thermodynamic limit only the leading $(Nm_*/2)^2$ term survives in both expressions, and identically for $\langle E_1|\hat{J}_z^2|E_1\rangle$, giving

$$G_{01} \xrightarrow{N \rightarrow \infty} \frac{(Nm_*)^2}{4}, \quad (22)$$

and since $G_{\text{loc}} = (Nm_*)^2/2$:

$$\eta_{\text{MF}}(N, \Gamma/J) \xrightarrow{N \rightarrow \infty} 2. \quad (23)$$

Geometric factors vs physical rates

Equation (23) is a statement about the *geometric factors* G_{loc} and G_{01} , not about physical dephasing rates in the thermodynamic limit. As $N \rightarrow \infty$, ΔE vanishes exponentially while $G_{01} \sim N^2$, so $2\Delta E \cdot T_2 \sim e^{-cN}/N^2 \rightarrow 0$: the secular approximation underlying $\gamma_\phi G_{01}$ breaks down. The physically meaningful regime is the mesoscopic secular window ($N \approx 250\text{--}430$, $\Gamma/J = 0.95$), where $2\Delta E \cdot T_2 \approx 18$ and both rates are well-defined exponential decay constants. The degenerate-limit physics is treated analytically in Section 3.4 below.

3.4 The degenerate limit: pointer basis and convergence of rates

As $N \rightarrow \infty$ and the doublet becomes degenerate, the secular approximation fails. The correct treatment is to diagonalise the Lindblad generator *within the degenerate subspace*. In the doublet $\{|E_0\rangle, |E_1\rangle\}$, the Parity Proposition (Section 6) forces $\langle E_i | \hat{J}_z | E_i \rangle = 0$, so \hat{J}_z is purely off-diagonal in the doublet subspace:

$$\hat{J}_z|_{\text{doublet}} = J_{01} \sigma_x, \quad (24)$$

where $J_{01} \equiv \langle E_0 | \hat{J}_z | E_1 \rangle$ and σ_x is the Pauli matrix in the $\{|E_0\rangle, |E_1\rangle\}$ basis. Note that using the exact definitions $|E_0\rangle = (|P\rangle + |R\rangle)/\sqrt{2}$ and $|E_1\rangle = (|P\rangle - |R\rangle)/\sqrt{2}$, one finds exactly for all N :

$$J_{01} = \langle E_0 | \hat{J}_z | E_1 \rangle = \frac{1}{2}(\langle P | + \langle R |) \hat{J}_z (|P\rangle - |R\rangle) = \frac{1}{2}(\langle P | \hat{J}_z | P \rangle - \langle R | \hat{J}_z | R \rangle).$$

In the thermodynamic limit, this expectation value approaches $\frac{Nm_*}{2}$, so that J_{01} is the same quantity as $\langle P | \hat{J}_z | P \rangle$ in the thermodynamic limit. This is not a notational accident: it reflects the fact that the off-diagonal Lindblad matrix element in the eigenstate basis equals the magnetisation of the pointer state, both converging to $Nm_*/2$ as $N \rightarrow \infty$ [1].

For \hat{J}_z^2 , the exact diagonal element within the full Hilbert space is:

$$\langle E_i | \hat{J}_z^2 | E_i \rangle = J_{01}^2 + \sum_{k \geq 2} |\langle E_i | \hat{J}_z | E_k \rangle|^2, \quad (25)$$

where the sum over $k \geq 2$ represents $\mathcal{O}(N)$ population leakage from the doublet into the higher Dicke states via the bath. Because G_{01} is the doublet average, we must account for both states: $|E_1\rangle$ sits closer to the barrier top and penetrates further into the classically forbidden region, producing significantly larger matrix elements with higher Dicke states than $|E_0\rangle$. Numerically, the average leakage accounts for $\approx 33.4\%$ at $N = 100$ (1.1% for E_0 vs 49.8% for E_1), $\approx 13.7\%$ at $N = 370$ (4.8% for E_0 vs 21.0% for E_1), and $\approx 3.4\%$ at $N = 1000$ of the total G_{01} . To obtain a self-contained dissipator within the doublet, we restrict to the low-energy manifold and set:

$$\hat{J}_z^2|_{\text{doublet}} = J_{01}^2 \mathbb{1}, \quad (26)$$

explicitly dropping the $k \geq 2$ leakage terms. This is physically justified because the internal doublet dephasing ($\mathcal{O}(N^2)$, set by G_{01}) dominates the leakage ($\mathcal{O}(N)$) by a factor $\sim N$ at large N ; the resulting error in the restricted Lindblad eigenvalues is $\mathcal{O}(N^{-1})$. The doublet description is therefore valid throughout the Goldilocks window where the gap ratio $(E_2 - E_0)/\Delta E \gg 1$ (Table 3); it is not claimed to be exact for the full many-body Hilbert space Lindbladian. The Lindblad dissipator restricted to the doublet is therefore:

$$\mathcal{D}[\rho]|_{\text{doublet}} = \gamma_\phi J_{01}^2 (\sigma_x \rho \sigma_x - \rho). \quad (27)$$

This is *dephasing in the σ_x eigenbasis*. The eigenstates of σ_x in the doublet are $|P\rangle = (|E_0\rangle + |E_1\rangle)/\sqrt{2}$ and $|R\rangle = (|E_0\rangle - |E_1\rangle)/\sqrt{2}$ — the pointer states selected by the bath [2].

The 4×4 Lindblad superoperator corresponding to Eq. (27) has spectrum:

$$\text{spec}(\mathcal{L})|_{\text{doublet}} = \gamma_\phi J_{01}^2 \times \{0, 0, -2, -2\}. \quad (28)$$

The two zero eigenvalues are the steady states *within the restricted doublet*: the total population $\text{tr}(\rho)$ and the pointer population difference $\rho_{PP} - \rho_{RR}$ (which equals $2\text{Re}(\rho_{01})$). The two eigenvalues $-2\gamma_\phi J_{01}^2$ govern the decaying modes: the eigenstate population difference $\rho_{00} - \rho_{11}$ and the imaginary part of the eigenstate coherence $\text{Im}(\rho_{01})$. Together, these decaying modes constitute the full complex pointer coherence ρ_{PR} , which decays strictly at $2\gamma_\phi J_{01}^2$.

Quasi-steady state vs. true steady state

Within the restricted 2-level doublet model, $\text{Re}(\rho_{01})$ is a zero eigenvalue of the doublet Lindblad superoperator and therefore a steady state of that restricted system. In the *full* $(N+1)$ -dimensional Hilbert space, however, the Lindblad operator \hat{J}_z couples the doublet to higher-energy Dicke states at rate $\gamma_\phi \times (\text{leakage}) \sim \gamma_\phi \mathcal{O}(N)$ (Section 3.4, Eq. (25)). The pure dephasing channel has no cooling: the system ultimately thermalises to the maximally mixed state over the full Hilbert space. $\text{Re}(\rho_{01})$ is therefore a *quasi-steady state* (metastable plateau): it remains approximately constant throughout the doublet-dephasing phase (of duration $\sim (\gamma_\phi G_{01})^{-1} \sim (\gamma_\phi N^2)^{-1}$, during which $\text{Im}(\rho_{01})$ and $\rho_{00} - \rho_{11}$ decay), and only decays on the much longer leakage timescale $(\gamma_\phi N)^{-1}$. The timescale separation $G_{01}/\text{leakage} \approx 7.3$ at $N = 370$ (from Table 3: $G_{01} = 2839$ vs. average leakage ≈ 388) ensures the doublet description remains physically well-defined for the mesoscopic secular window. All rate formulas in this paper are valid at intermediate times $(\gamma_\phi N^2)^{-1} \ll t \ll (\gamma_\phi N)^{-1}$.

Since $|P\rangle \equiv (|E_0\rangle + |E_1\rangle)/\sqrt{2}$ by definition, $|E_0\rangle = (|P\rangle + |R\rangle)/\sqrt{2}$ is an exact algebraic identity for all N , so $J_{01} = \langle P|\hat{J}_z|P\rangle$ exactly. As $N \rightarrow \infty$, $|\tilde{P}\rangle \rightarrow |P\rangle$ (correction $\mathcal{O}(S) \rightarrow 0$), giving $J_{01} \rightarrow Nm_*/2$, and:

$$J_{01}^2 \xrightarrow{N \rightarrow \infty} \left(\frac{Nm_*}{2}\right)^2 = G_{01}. \quad (29)$$

The doubly-degenerate nonzero decay rate therefore satisfies:

$$2\gamma_\phi J_{01}^2 \xrightarrow{N \rightarrow \infty} 2\gamma_\phi G_{01} = \gamma_\phi G_{\text{loc}}. \quad (30)$$

The decaying components of both coherences are governed by $\gamma_\phi G_{\text{loc}}$ in the thermodynamic limit. Numerical verification is shown in Figure 3.

Three-regime structure

The physical content of $\eta_{\text{MF}} = G_{\text{loc}}/G_{01}$ is organised into three regimes:

Regime 1 — Small N ($N \lesssim 100$): The double-well is not yet established ($Nm_* \lesssim 30$). $\eta_{\text{MF}} < 2$ and can fall below 1. Neither rate formula gives a well-defined exponential decay constant: $G_{\text{loc}} = (Nm_*)^2/2$ overestimates the actual order parameter because the mean-field value m_* is not yet established at finite N , while G_{01} loses meaning as the doublet is not spectrally isolated from higher states (gap ratio $\lesssim 3$, Table 3) and

the SCS approximation has relative error $\gtrsim 9\%$.

Regime 2 — Mesoscopic secular window ($N \approx 250\text{--}430$): The secular condition $2\Delta E \cdot T_2 \gg 1$ is satisfied (≈ 18.4 at $N = 370$) and the doublet is well-isolated from higher states (gap ratio $(E_2 - E_0)/\Delta E \approx 11.4$). Two coherences with *genuinely different* exponential decay rates:

$$\dot{\rho}_{01}|_{\text{diss}} = -\gamma_\phi G_{01} \rho_{01}, \quad \dot{\rho}_{PR}|_{\text{diss}} \simeq -\gamma_\phi G_{\text{loc}} \rho_{PR}, \quad \eta_{\text{MF}} \approx 2.35\text{--}2.40.$$

This is the protected quantum regime. It encompasses the thermal ‘‘Goldilocks’’ zone ($N \approx 250\text{--}370$) defined in the companion paper [1] — demonstrating that the dynamical protection of the secular approximation outlasts the strict thermal bounds, allowing quantum technologies to harvest a coherence lifetime extended by a factor of $\eta_{\text{exact}} \approx 1.86$ (exact physical protection) or a factor of $\eta_{\text{MF}} \approx 2.35\text{--}2.40$ (advantage over classical mean-field).

Regime 3 — Thermodynamic limit ($N \rightarrow \infty$): The secular approximation fails ($\Delta E \rightarrow 0$, doublet degenerate). The Lindblad generator in the doublet is Eq. (27), with the doubly-degenerate nonzero rate $2\gamma_\phi J_{01}^2 \rightarrow \gamma_\phi G_{\text{loc}}$. The pointer coherence ρ_{PR} and $\text{Im}(\rho_{01})$ decay at $\gamma_\phi G_{\text{loc}}$; $\text{Re}(\rho_{01})$ approaches a quasi-steady plateau within the doublet (true steady state only in the doublet approximation; it decays on the longer leakage timescale $\sim (\gamma_\phi N)^{-1}$ in the full Hilbert space). *The two pictures converge*. The factor of η_{MF} is a *mesoscopic quantum effect*, not a universal constant.

The factor of 2 has a precise physical origin. G_{loc} is *half* the squared distance between macroscopic magnetisations: $G_{\text{loc}} = (\langle P|\hat{J}_z|P\rangle - \langle R|\hat{J}_z|R\rangle)^2/2 = (Nm_*)^2/2 = 2(Nm_*/2)^2$. Note that $\langle P|\hat{J}_z^2|P\rangle \rightarrow (Nm_*/2)^2$ and $\langle E_0|\hat{J}_z^2|E_0\rangle \rightarrow (Nm_*/2)^2$ converge to the same value individually — their ratio approaches 1, not 2. For the eigenstate, this $\mathcal{O}(N^2)$ variance is not standard statistical noise, but the macroscopic quantum uncertainty of a superposition between $+Nm_*/2$ and $-Nm_*/2$. The factor of 2 arises because G_{loc} is *twice* this single-state variance: it measures the squared distance between two states, not the variance of one. In the localised basis, the cross-term $\langle P|\hat{J}_z|P\rangle\langle R|\hat{J}_z|R\rangle = -(Nm_*/2)^2$ doubles the rate; in the eigenstate basis, the analogous cross-term $\langle E_0|\hat{J}_z|E_0\rangle\langle E_1|\hat{J}_z|E_1\rangle = 0$ exactly by parity, for all N .

4 Finite- N Amplification

At finite N the mean-field ratio η_{MF} has a richer structure. For very small N , where the double-well structure is not yet well-developed and the eigenstates are delocalised ($Nm_* \ll 1$), the eigenstate second moment $\langle E_i|\hat{J}_z^2|E_i\rangle$ exceeds $(Nm_*/2)^2$: $\eta_{\text{MF}} < 1$. As N increases into the ordered phase, η_{MF} passes through 1 (around $N \approx 25\text{--}30$ at $\Gamma/J = 0.95$), rises to a maximum $\eta_{\text{MF,peak}} \approx 2.40$ near $N \approx 300$, then decreases monotonically toward $\eta_{\text{MF}} = 2$ as $N \rightarrow \infty$.

The amplification above 2 at finite N has a precise origin: $\langle E_i|\hat{J}_z^2|E_i\rangle$ is suppressed below $(Nm_*/2)^2$ by quantum fluctuations as the eigenstate wavefunction spreads into the classically forbidden region near $m_z = 0$:

$$G_{01} = \left(\frac{Nm_*}{2}\right)^2 - \delta G(N, \Gamma/J), \quad \delta G \sim \mathcal{O}(N). \quad (31)$$

Hence $\eta_{\text{MF}} = 2 + \mathcal{O}(N^{-1})$, with the correction largest near the crossover $\Delta E \approx k_B T$ [1],

where the wavefunction spread is maximum.

5 The LMG Model: Exact Numerics

The Lipkin-Meshkov-Glick Hamiltonian [6, 16] is the N -spin realisation of Eq. (3), exactly solvable by diagonalisation of the $(N + 1)$ -dimensional symmetric Dicke sector.

5.1 The ratio $\eta_{\text{MF}}(N, \Gamma/J)$

Figure 1 shows η_{MF} versus N at $\Gamma/J = 0.95$.

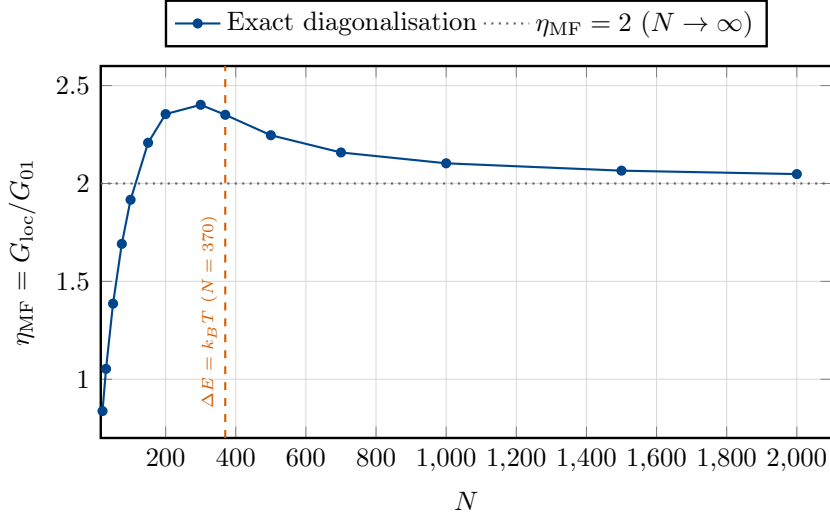


Figure 1. Ratio $\eta_{\text{MF}} = G_{\text{loc}}/G_{01}$ versus N at $\Gamma/J = 0.95$, from exact diagonalisation. $\eta_{\text{MF}} < 1$ for small N (double-well not yet developed); peaks at $\eta_{\text{MF}} \approx 2.40$ near $N = 300$; decreases toward the geometric lower bound $\eta_{\text{MF}} = 2$ (dotted). The crossover $\Delta E = k_B T$ (dashed red) sits at $N = 370$.

Table 3 lists the key values. The $N \rightarrow \infty$ row gives the analytic thermodynamic-limit result.

Table 3. Dimensionless geometric factors $G_{\text{loc}} \equiv (Nm_*)^2/2$ and $G_{01} \equiv \frac{1}{2}(\langle E_0 | \hat{J}_z^2 | E_0 \rangle + \langle E_1 | \hat{J}_z^2 | E_1 \rangle)$ at $\Gamma/J = 0.95$ ($m_* = 0.312$). The mean-field dephasing rate is $\gamma_\phi G_{\text{loc}}$; the exact eigenstate rate is $\gamma_\phi G_{01}$. The ratio η_{MF} is independent of γ_ϕ . The gap ratio $(E_2 - E_0)/\Delta E$ quantifies doublet isolation from higher states. The secular parameter $2\Delta E \cdot T_2$ is evaluated at the benchmark $\gamma_\phi = 0.05 \text{ s}^{-1}$ [1]; values $\gg 1$ confirm the secular approximation; values $\lesssim 3$ indicate its breakdown. All entries are computed from full-precision exact diagonalisation and rounded independently; small inconsistencies in the last displayed digit (e.g. $488/254 = 1.921$ vs $\eta_{\text{MF}} = 1.917$ at $N = 100$) reflect this independent rounding.

N	$\Delta E/k_B T$	G_{loc}	G_{01}	η_{MF}	$(E_2 - E_0)/\Delta E$	$2\Delta E T_2$
100	7.33	488	254	1.917	3.0	1510
200	3.63	1950	828	2.354	4.1	230
300	1.75	4388	1827	2.402	6.9	50
370	1.00	6674	2839	2.351	11.4	18
500	0.32	12188	5425	2.246	37.3	3
1000	$\ll 1$	48750	23180	2.103	$> 10^3$	$\ll 1$
2000	$\ll 1$	195000	95214	2.048	$> 10^3$	$\ll 1$
∞	0	$N^2 m_*^2/2$	$N^2 m_*^2/4$	2	∞	0

5.2 Dependence on Γ/J

Figure 2 shows η_{MF} versus Γ/J at $N = 370$.

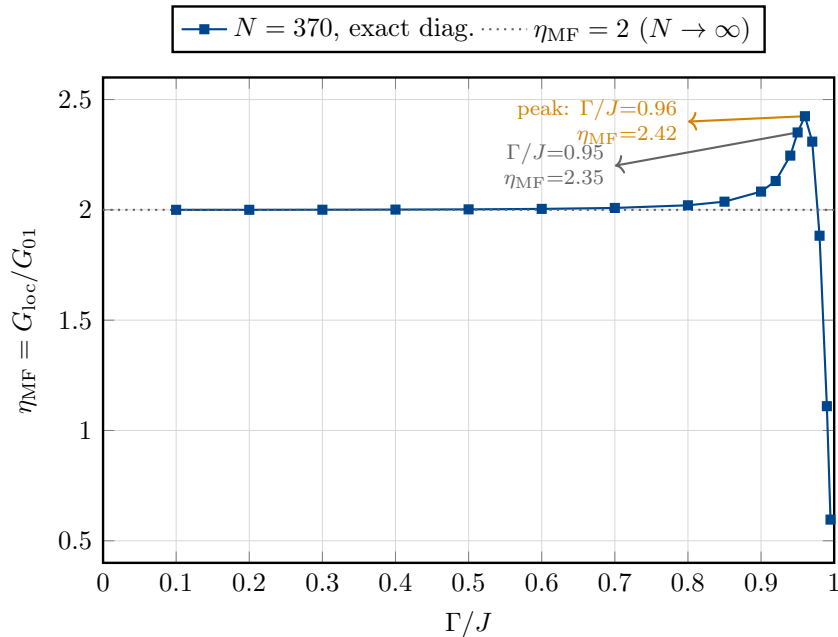


Figure 2. Ratio η_{MF} versus Γ/J at $N = 370$. $\eta_{\text{MF}} \rightarrow 2$ deep in the ordered phase ($\Gamma/J \rightarrow 0$); maximum $\eta_{\text{MF}} \approx 2.42$ at $\Gamma/J \approx 0.96$ (orange arrow); benchmark $\Gamma/J = 0.95$ marked (grey arrow). η_{MF} falls sharply through 1 and approaches 0 near criticality.

5.3 Convergence: geometric factors and physical rates

Fitting $\eta_{\text{MF}}(N) = 2 + c/N$ at $\Gamma/J = 0.95$ gives $c \approx 123$ at $N = 500$, decreasing to $c \approx 103$ at $N = 1000$ and $c \approx 96$ at $N = 2000$, confirming the $\mathcal{O}(N^{-1})$ approach of the geometric ratio to 2. The factor of 2 in η_{MF} is not a finite- N artefact.

However, the geometric convergence $\eta_{\text{MF}} \rightarrow 2$ is not the same as the convergence of physical rates. As established in Section 3.4, the full Lindblad superoperator in the degenerate doublet has a doubly-degenerate nonzero eigenvalue $2\gamma_\phi J_{01}^2$, which converges to $\gamma_\phi G_{\text{loc}}$ from below. Simultaneously, the secular rate $\gamma_\phi G_{01}$ converges to $\gamma_\phi G_{\text{loc}}/2$. Both physical rates therefore converge to $\gamma_\phi G_{\text{loc}}$; $\eta_{\text{MF}} \rightarrow 2$ is the geometric expression of this convergence.

Figure 3 shows all three rates normalised by the common scale $(Nm_*/2)^2$, making the convergence visually explicit.

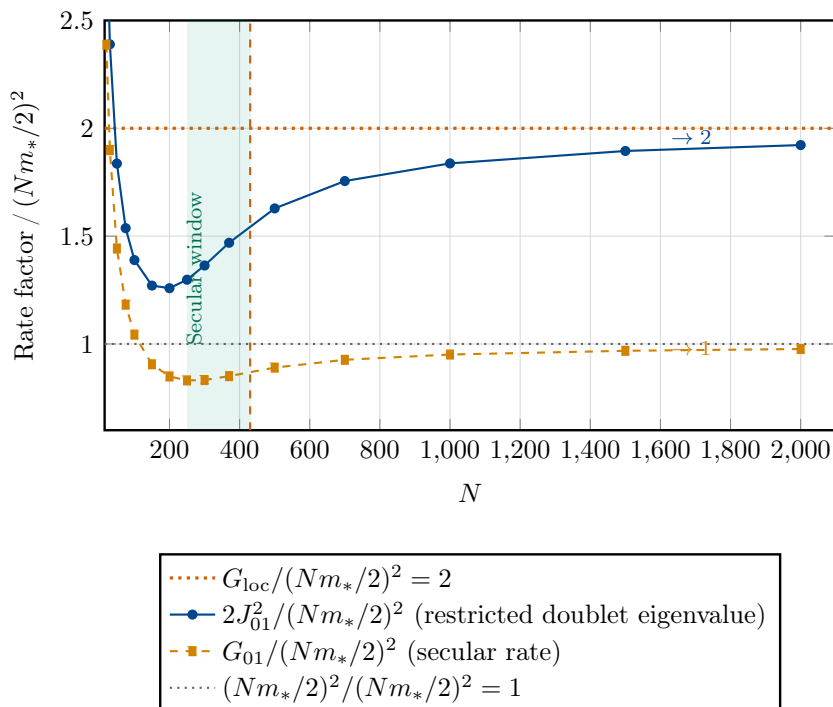


Figure 3. Three decoherence rate factors normalised by $(Nm_*/2)^2$, the single-state second moment in the thermodynamic limit. *Red dotted* (flat at 2): $G_{\text{loc}}/(Nm_*/2)^2 = 2$, the localised-state rate — constant by definition. *Blue solid*: $2J_{01}^2/(Nm_*/2)^2$, the nonzero eigenvalue of the restricted doublet Lindblad superoperator (Eq. (28)); *converges to 2*, i.e. merges with $\gamma_\phi G_{\text{loc}}$, as $N \rightarrow \infty$, confirming Eq. (30). *Orange dashed*: $G_{01}/(Nm_*/2)^2 = 2/\eta_{\text{MF}}$, the secular rate; *converges to 1*, i.e. to $\gamma_\phi G_{\text{loc}}/2$ — does *not* merge with the other two curves. The factor $\eta_{\text{MF}} = G_{\text{loc}}/G_{01} \rightarrow 2$ is the ratio between the red and orange asymptotes. The shaded region is the mesoscopic secular window ($2\Delta E \cdot T_2 \gg 1$), the only regime where both rates are simultaneously well-defined exponential decay constants. This dynamically protected window comfortably encompasses the narrower thermal “Goldilocks” zone ($N \approx 250\text{--}370$, $\Delta E \gtrsim k_B T$) required for experimental protocols [1].

6 Parity Proposition

The vanishing of the cross-term in the eigenstate basis is an exact consequence of the \mathbb{Z}_2 symmetry.

Proposition. *Let $[\hat{H}, \hat{P}] = 0$ and $\hat{P}\hat{L}\hat{P}^\dagger = -\hat{L}$, where \hat{P} is a unitary operator ($\hat{P}^\dagger\hat{P} = \mathbb{1}$). Then for any eigenstate $|E_i\rangle$ of \hat{H} with $\hat{P}|E_i\rangle = p_i|E_i\rangle$: $\langle E_i|\hat{L}|E_i\rangle = 0$.*

Proof. Inserting $\hat{P}^\dagger\hat{P} = \mathbb{1}$ on both sides of \hat{L} :

$$\begin{aligned}\langle E_i|\hat{L}|E_i\rangle &= \langle E_i|\hat{P}^\dagger \underbrace{(\hat{P}\hat{L}\hat{P}^\dagger)}_{=-\hat{L}} \hat{P}|E_i\rangle \\ &= p_i^* \cdot (-1) \cdot p_i \langle E_i|\hat{L}|E_i\rangle.\end{aligned}\tag{32}$$

Since \hat{P} is unitary, $|p_i|^2 = 1$, so $p_i^*p_i = 1$, and therefore $\langle E_i|\hat{L}|E_i\rangle = -\langle E_i|\hat{L}|E_i\rangle$, hence $\langle E_i|\hat{L}|E_i\rangle = 0$. \square

Note on the LMG implementation. With $\hat{P} = e^{i\pi\hat{J}_x}$, the operator is unitary for all N and satisfies $e^{i\pi\hat{J}_x}\hat{J}_ze^{-i\pi\hat{J}_x} = -\hat{J}_z$. For even N , $\hat{P}^2 = \mathbb{1}$ and \hat{P} is Hermitian with eigenvalues $p_i = \pm 1$. For odd N , $\hat{P}^2 = -\mathbb{1}$ and the eigenvalues are $p_i = \pm i$; the Proposition still holds since only $|p_i|^2 = 1$ is required. All numerical examples in this paper use even N , for which \hat{P} is Hermitian. The alternative choice $\hat{P} = \prod_j \hat{\sigma}_j^x$ is Hermitian and satisfies $\hat{P}^2 = \mathbb{1}$ for all N . The commutation $[\hat{H}, \hat{P}] = 0$ holds for the zero longitudinal field Hamiltonian of Eq. (3) and can be verified directly: $e^{i\pi\hat{J}_x}(-\frac{2J}{N}\hat{J}_z^2 - 2\Gamma\hat{J}_x)e^{-i\pi\hat{J}_x} = -\frac{2J}{N}\hat{J}_z^2 - 2\Gamma\hat{J}_x = \hat{H}$, using $e^{i\pi\hat{J}_x}\hat{J}_ze^{-i\pi\hat{J}_x} = -\hat{J}_z$ and $e^{i\pi\hat{J}_x}\hat{J}_xe^{-i\pi\hat{J}_x} = +\hat{J}_x$.

Corollary 1 (Population-coherence decoupling for opposite-parity pairs). For $i \neq j$ with $p_i^*p_j \neq 1$ (opposite parity eigenvalues), the Redfield tensor element coupling the population ρ_{ii} to the coherence ρ_{ij} evaluates to:

$$R_{(ii),(ij)} = \gamma_\phi \langle E_i|\hat{J}_z|E_i\rangle \langle E_j|\hat{J}_z|E_i\rangle - \frac{\gamma_\phi}{2} \langle E_j|\hat{J}_z^2|E_i\rangle.\tag{33}$$

Within the Markovian Lindblad dissipator used here, $R_{(ii),(ij)} = 0$ exactly: populations and coherences between states of opposite parity decouple without secular approximation. This decoupling is exact for the flat-spectrum Lindblad form of Eq. (9); it need not hold for a general microscopic Redfield tensor with frequency-dependent spectral density. The first term in $R_{(ii),(ij)}$ vanishes by the Proposition ($\langle E_i|\hat{J}_z|E_i\rangle = 0$); the second term $\langle E_j|\hat{J}_z^2|E_i\rangle = 0$ because \hat{J}_z^2 is parity-even and cannot connect states of opposite parity. For same-parity pairs ($p_i = p_j$), $\langle E_j|\hat{J}_z^2|E_i\rangle \neq 0$ in general and the decoupling does not hold. The ground doublet ($p_0 = +1$, $p_1 = -1$) is the opposite-parity case: the decoupling of ρ_{01} from populations is exact.

Corollary 2 (Secular approximation for ρ_{01}). The secular approximation for ρ_{01} drops the term $\gamma_\phi |\langle E_0|\hat{J}_z|E_1\rangle|^2$ coupling ρ_{01} to ρ_{10} . In the interaction picture, this coupling oscillates at $2\Delta E/\hbar$ (the counter-rotation of ρ_{01} and ρ_{10}); the secular condition is $(2\Delta E/\hbar) \cdot T_2 \gg 1$, where $T_2 \equiv (\gamma_\phi G_{01})^{-1}$ is as defined in Section 3. At the LMG benchmark, $(2\Delta E/\hbar) \cdot T_2 \approx 18.4$ [1]. This term does not vanish by parity: \hat{J}_z is parity-odd and $\langle E_0|\hat{J}_z|E_1\rangle \neq 0$.

The proposition holds for any system with $[\hat{H}, \hat{P}] = 0$ and $\hat{P}\hat{L}\hat{P}^\dagger = -\hat{L}$: spin-boson models in the broken-symmetry phase, the Dicke model in the superradiant phase, molecular aggregates with H- or J-type symmetry, two-mode BECs [5].

7 Implications

7.1 Quantum metrology and spin squeezing

The quantum Fisher information $F_Q[\rho, \hat{J}_z]$ and the Wineland spin-squeezing parameter ξ^2 are sensitive to the eigenstate coherence ρ_{01} , not to ρ_{PR} , when the system dynamics are effectively restricted to the ground-state doublet (as in the mesoscopic window where the gap to $|E_2\rangle$ is $\approx 11.4 \times \Delta E$ [1]). In general, QFI and squeezing depend on the full covariance matrix of the collective spins; the doublet restriction is the regime in which the present results apply directly. Consequently, quantum sensors operating in this mesoscopic window are affected by the slower eigenstate rate $\gamma_\phi G_{01}$ rather than the exact pointer-state rate $\gamma_\phi(G_{01} + J_{01}^2)$, giving a coherence lifetime longer by a factor of $\eta_{\text{exact}} \in [1, 1.86]$ compared to the pointer basis. Against the classical mean-field estimate $\gamma_\phi G_{\text{loc}}$, the advantage is the larger factor $\eta_{\text{MF}} \in [2, 2.42]$, provided the dynamics remain effectively confined to the ground-state doublet. This protection is operationally defined: for protocols that initialise, manipulate, and measure within the energy eigenbasis, the relevant decoherence rate is $\gamma_\phi G_{01}$, which is slower than the localised-state rate $\gamma_\phi G_{\text{loc}}$ by the factor η_{MF} . This is not merely a choice of basis — it reflects the physical suppression of dephasing channels by the \mathbb{Z}_2 parity symmetry (Proposition, Section 6), which forces the diagonal matrix elements of the Lindblad jump operator, $\langle E_i | \hat{J}_z | E_i \rangle = 0$ exactly, eliminating the cross-term that doubles the localised rate. The correct physical decoherence rate is $\gamma_\phi G_{01}$, with G_{01} given in Eq. (11).

7.2 Leggett-Garg inequality tests

In the companion paper [1], the Leggett-Garg correlator K_3 exhibits a robust violation $K_3 \approx 1.32$ at $\gamma_\phi \lesssim 0.289 \text{ s}^{-1}$ ($N = 370$, $\Gamma/J = 0.95$). This threshold is set by G_{01} , not G_{loc} . Using the mean-field estimate $\gamma_\phi G_{\text{loc}}$ in place of $\gamma_\phi G_{01}$ would predict a Level A threshold of $\gamma_\phi \lesssim 0.050 \text{ s}^{-1}$ — a factor of $\eta_{\text{MF}} = 2.35 \times$ below the correct two-level eigenstate threshold of 0.117 s^{-1} (Level B, this paper). The further factor from multi-level Lindblad effects (Level B to Level C in Ref. [1]) brings the total up to $5.8 \times$ enhancement compared to mean-field estimates: $5.8 \times = 2.35 \times$ (parity cross-term, this paper) $\times 2.47 \times$ (additional odd-parity Dicke states). These factors are computed from full-precision values ($\gamma_\phi^{(\text{B})} = 0.1173 \text{ s}^{-1}$, $\gamma_\phi^{(\text{A})} = 0.0499 \text{ s}^{-1}$) and rounded independently; multiplying the rounded figures introduces a residual discrepancy of $\lesssim 0.5\%$. These contributions are physically distinct and independently computable.

7.3 General collective spin systems

The result applies to anisotropic collective spin models (such as the infinite-range Ising or anisotropic Heisenberg models), the Dicke model in the superradiant phase, two-mode BECs in the broken-symmetry phase [5], and molecular aggregates with site-exchange symmetry. In each case the exact pointer-state rate exceeds the eigenstate rate by a factor of $\eta_{\text{exact}} \in [1, \eta_{\text{exact,peak}}]$, and the mean-field estimate exceeds it by a factor of $\eta_{\text{MF}} \in [2, \eta_{\text{MF,peak}}]$, where the thermodynamic lower bound $\eta_{\text{MF}} = 2$ is universal (Section 3.3) but the finite- N peaks are model-dependent and must be computed from the specific instanton action and crossover dynamics of the system in question.

8 Discussion

The central point is simple: *if your protocol initialises and measures in the energy eigenstate basis, use $\gamma_\phi G_{01}$. If your protocol uses localised order-parameter states, use $\gamma_\phi G_{\text{loc}}$. They are not the same.*

The factor of 2 between them in the thermodynamic limit is the ratio of half the squared distance between macroscopic first moments, $(Nm_*)^2/2$, to the eigenstate variance $(Nm_*/2)^2$. It is not the ratio of two second moments (both $\langle P|\hat{J}_z^2|P\rangle$ and $\langle E_0|\hat{J}_z^2|E_0\rangle$ converge to $(Nm_*/2)^2$ individually; their ratio approaches 1); it is the factor by which half the squared distance exceeds the single-state variance. The cross-term $\langle P|\hat{J}_z|P\rangle\langle R|\hat{J}_z|R\rangle = -(Nm_*/2)^2$ in the localised basis doubles the rate; the analogous term vanishes exactly in the eigenstate basis by parity.

The basis dependence of the rates — how can the same physical system have two different decoherence rates? — is clarified by the three-regime structure of Section 3.4: the two rates correspond to different observables (the order-parameter coherence ρ_{PR} and the energy-eigenstate coherence ρ_{01}) and are not in contradiction. In the thermodynamic limit, the degenerate doublet analysis shows that the decaying components of both coherences are governed by $\gamma_\phi G_{\text{loc}}$: $\text{Re}(\rho_{01})$ becomes a quasi-steady state and the remainder decays at the doubly-degenerate nonzero Lindblad eigenvalue $2\gamma_\phi J_{01}^2 \rightarrow \gamma_\phi G_{\text{loc}}$. The rate difference exists only in the mesoscopic secular window where $\Delta E > 0$ renders the secular approximation valid and the two coherences genuinely distinct.

This is precisely where quantum protocols sensitive to ρ_{01} are most affected. For such protocols — those initialised, manipulated, and read out within the energy eigenbasis, with dynamics effectively confined to the ground-state doublet — the mesoscopic secular window provides an operational coherence lifetime longer by a factor of $\eta_{\text{exact}} \lesssim 2$ (specifically ≈ 1.86 at the benchmark) compared to the exact pointer-state decay rate, or up to a factor of $\eta_{\text{MF}} \approx 2.42$ compared to the classical mean-field estimate $\gamma_\phi G_{\text{loc}}$.

The structure $\langle \hat{J}_z \rangle_{|P\rangle} \xrightarrow{N \rightarrow \infty} Nm_*/2$ (which diverges as $N \rightarrow \infty$) while $\langle \hat{J}_z \rangle_{|E_0\rangle} = 0$ exactly by parity reflects the fundamental difference between statistical variance and macroscopic quantum uncertainty. In the localised state, the variance is standard statistical noise $\mathcal{O}(N)$; in the symmetric eigenstate, the $\mathcal{O}(N^2)$ variance is the signature of a macroscopic Schrödinger cat state. The factor of 2 isolates this distinction. The mesoscopic secular window is the finite-system analogue of the regime where spontaneous symmetry breaking produces physical observables distinct from those of the symmetric phase.

At finite N near the crossover, the mean-field ratio reaches $\eta_{\text{MF}} \approx 2.35$ – 2.42 and the exact physical protection factor $\eta_{\text{exact}} \approx 1.86$, precisely where quantum protocols are most sensitive. The Proposition of Section 6 is elementary; its consequences for decoherence calculations in symmetry-broken phases are not.

Acknowledgements

This work builds on the framework of Ref. [1].

A Numerical Methods

All matrix elements are computed by exact diagonalisation of the LMG Hamiltonian in the symmetric Dicke sector $\{|J_t, m\rangle : m = -J_t, \dots, +J_t\}$, $J_t = N/2$. The $(N+1) \times (N+1)$ Hamiltonian is tridiagonal with diagonal elements $-2Jm^2/N$ and off-

diagonal elements $-\Gamma\sqrt{J_t(J_t+1)-m(m+1)}$. Diagonalisation uses `scipy.linalg.eigh` (LAPACK `dsyevd` backend) in double-precision floating point (`float64`). Matrix elements $\langle E_i|\hat{J}_z^2|E_i\rangle$ and $\langle E_i|\hat{J}_z|E_j\rangle$ are extracted directly from the eigenvector coefficients in the Dicke basis. Numerical convergence was validated by verifying: (i) the completeness relation $\sum_k |\langle E_i|\hat{J}_z|E_k\rangle|^2 = \langle E_i|\hat{J}_z^2|E_i\rangle$ (to machine precision, $\sim 10^{-12}$, for all N in Table 3); (ii) the parity symmetry $\langle E_i|\hat{J}_z|E_i\rangle = 0$ (satisfied to $\sim 10^{-14}$ for all even-parity eigenstates); (iii) the $\eta_{\text{MF}}(N) = 2 + c/N$ scaling, confirmed by the fit $c \approx 103$ at $N = 1000$ and $c \approx 96$ at $N = 2000$. For $N = 2000$, the $(2001) \times (2001)$ matrix is diagonalised in ~ 10 s on a standard workstation; no convergence issues were observed. The companion paper [1] provides the full self-tested simulation code at <https://arxiv.org/abs/2604.18638>.

B Derivation of the Two-Channel Decay Structure

This appendix provides a self-contained derivation of the decay structure of ρ_{PR} in the localised basis, resolving the two coupled channels identified in Section 3.

B.1 Full projection of the Lindblad equation

We restrict the dynamics to the 2D projected density matrix within the pointer-state doublet $\{|P\rangle, |R\rangle\}$. We explicitly parameterise the complex coherence as $\rho_{PR} = u + iv$, where:

$$u \equiv \text{Re}(\rho_{PR}), \quad v \equiv \text{Im}(\rho_{PR}), \quad w \equiv \rho_{PP} - \rho_{RR}. \quad (34)$$

These three real quantities, alongside the conserved trace $\rho_{PP} + \rho_{RR} = 1$, fully characterise the doublet density matrix, which can be written visually as:

$$\rho = \begin{pmatrix} \rho_{PP} & \rho_{PR} \\ \rho_{RP} & \rho_{RR} \end{pmatrix} = \begin{pmatrix} \frac{1+w}{2} & u + iv \\ u - iv & \frac{1-w}{2} \end{pmatrix}. \quad (35)$$

Hamiltonian contribution

The LMG Hamiltonian restricted to the doublet acts as $\hat{H}|_{\text{doublet}} = -(\Delta E/2)\sigma_x$ in the $\{|P\rangle, |R\rangle\}$ basis (with energy zero shifted to the doublet midpoint). The Hamiltonian evolution $\dot{\rho}|_{\text{H}} = -i[\hat{H}, \rho]$ evaluates to the matrix:

$$\dot{\rho}|_{\text{H}} = i\frac{\Delta E}{2}[\sigma_x, \rho] = \begin{pmatrix} \Delta E \cdot v & -i\frac{\Delta E}{2} \cdot w \\ i\frac{\Delta E}{2} \cdot w & -\Delta E \cdot v \end{pmatrix}. \quad (36)$$

Equating matrix elements with $\dot{\rho} = \begin{pmatrix} \dot{\rho}_{PP} & \dot{u} + i\dot{v} \\ \dot{u} - i\dot{v} & \dot{\rho}_{RR} \end{pmatrix}$, we extract the components:

$$\dot{u}|_{\text{H}} = 0, \quad (37)$$

$$\dot{v}|_{\text{H}} = -\frac{\Delta E}{2} \cdot w, \quad (38)$$

$$\dot{w}|_{\text{H}} = \dot{\rho}_{PP} - \dot{\rho}_{RR} = +2\Delta E \cdot v. \quad (39)$$

Dissipator contribution

Using the SCS approximation for the pointer-state matrix elements ($\langle P|\hat{J}_z|P\rangle = +Nm_*/2$, $\langle P|\hat{J}_z^2|P\rangle \simeq (Nm_*/2)^2$) and the exact parity result $\langle P|\hat{J}_z|R\rangle = 0$, the dissipator exclusively

suppresses the off-diagonal coherences at the rate $\gamma_\phi G_{\text{loc}}$:

$$\dot{\rho}|_{\text{D}} = \begin{pmatrix} 0 & -\gamma_\phi G_{\text{loc}} \rho_{PR} \\ -\gamma_\phi G_{\text{loc}} \rho_{RP} & 0 \end{pmatrix} = \begin{pmatrix} 0 & -\gamma_\phi G_{\text{loc}} (u + iv) \\ -\gamma_\phi G_{\text{loc}} (u - iv) & 0 \end{pmatrix}. \quad (40)$$

This yields:

$$\dot{u}|_{\text{D}} = -\gamma_\phi G_{\text{loc}} u, \quad (41)$$

$$\dot{v}|_{\text{D}} = -\gamma_\phi G_{\text{loc}} v, \quad (42)$$

$$\dot{w}|_{\text{D}} = 0. \quad (43)$$

The dissipator does not change the population difference w at leading order (the localised states are steady states of the dissipator in the limit $Nm_* \gg 1$).

Combined equations and Channel Separation

Collecting the Hamiltonian and dissipator contributions, the full dynamics can be written intuitively as a matrix differential equation for the real vector $(u, v, w)^T$:

$$\frac{d}{dt} \begin{pmatrix} u \\ v \\ w \end{pmatrix} = \begin{pmatrix} -\gamma_\phi G_{\text{loc}} & 0 & 0 \\ 0 & -\gamma_\phi G_{\text{loc}} & -\Delta E/2 \\ 0 & +2\Delta E & 0 \end{pmatrix} \begin{pmatrix} u \\ v \\ w \end{pmatrix}. \quad (44)$$

Written in this visual form, the channel separation is immediate: the u component (the real part of the coherence) is completely block-diagonalized and decays independently, while the v and w components form a coupled two-dimensional subsystem.

B.2 Channel separation

From equation (44) we can see that u decouples completely: $u = \text{Re}(\rho_{PR})$ undergoes pure exponential decay at the localised rate:

$$u(t) = u(0) e^{-\gamma_\phi G_{\text{loc}} t}. \quad (45)$$

This is the channel captured by Eq. (15) in the main text.

The lower parts of the block diagonal matrix of equation (44) form a coupled 2×2 linear system for (v, w) . The characteristic polynomial of the matrix $M = \begin{pmatrix} -\gamma_\phi G_{\text{loc}} & -\Delta E/2 \\ +2\Delta E & 0 \end{pmatrix}$ (with $\det M = \Delta E^2$ and $\text{tr} M = -\gamma_\phi G_{\text{loc}}$) is:

Remark 1. The off-diagonal coupling coefficients $-\Delta E/2$ and $+2\Delta E$ are asymmetric. This is because $v = \text{Im}(\rho_{PR})$ is a coherence element (dimensionless amplitude) while $w = \rho_{PP} - \rho_{RR}$ is a population difference (also dimensionless but with different normalisation conventions in the Bloch picture). The factors are verified numerically by direct computation of $-i[\hat{H}, \rho]$ for the doublet Hamiltonian $\hat{H}|_{\text{doublet}} = -(\Delta E/2)\sigma_x$; the characteristic polynomial $\det(M - \lambda \mathbb{1}) = \lambda^2 + \gamma_\phi G_{\text{loc}} \lambda + \Delta E^2 = 0$ is correct.

$$\lambda^2 + \gamma_\phi G_{\text{loc}} \lambda + \Delta E^2 = 0, \quad (46)$$

with roots:

$$\lambda_{\pm} = -\frac{\gamma_\phi G_{\text{loc}}}{2} \pm \sqrt{\left(\frac{\gamma_\phi G_{\text{loc}}}{2}\right)^2 - \Delta E^2}. \quad (47)$$

B.3 Two regimes

Overdamped / quantum Zeno regime ($\gamma_\phi G_{\text{loc}} \gg 2\Delta E$)

The discriminant is positive. Both roots are real and negative: $\lambda_+ \approx -\Delta E^2/(\gamma_\phi G_{\text{loc}})$ (slow) and $\lambda_- \approx -\gamma_\phi G_{\text{loc}}$ (fast). The slow root gives a decay rate:

$$\Gamma_{\text{slow}} \approx \frac{\Delta E^2}{\gamma_\phi G_{\text{loc}}} = \frac{\Delta E^2}{2\gamma_\phi G_{01}} \cdot \frac{G_{01}}{G_{\text{loc}}/2} \ll \gamma_\phi G_{01}. \quad (48)$$

In this regime the strong bath suppresses tunnelling (quantum Zeno effect), and the effective decay of v and w is algebraically slow.

Underdamped / secular regime ($\Delta E \gg \gamma_\phi G_{\text{loc}}$, *the mesoscopic window*)

The discriminant is negative. The roots are complex:

$$\lambda_{\pm} = -\frac{\gamma_\phi G_{\text{loc}}}{2} \pm i\Delta E, \quad (49)$$

giving:

$$v(t) \propto e^{-(\gamma_\phi G_{\text{loc}}/2)t} \cos(\Delta E t + \phi_0), \quad (50)$$

and similarly for $w(t)$. The solution is a *damped oscillation* at frequency ΔE with amplitude envelope decaying at:

$$\Gamma_{\text{env}} = \frac{\gamma_\phi G_{\text{loc}}}{2} = \gamma_\phi \frac{(Nm_*)^2}{4}. \quad (51)$$

Comparing with G_{01} :

$$\frac{\Gamma_{\text{env}}}{\gamma_\phi G_{01}} = \frac{G_{\text{loc}}/2}{G_{01}} = \frac{\eta_{\text{MF}}}{2} \xrightarrow{N \rightarrow \infty} 1. \quad (52)$$

The envelope rate $\gamma_\phi G_{\text{loc}}/2$ equals $\gamma_\phi G_{01}$ only in the thermodynamic limit $\eta_{\text{MF}} \rightarrow 2$; at finite N it exceeds $\gamma_\phi G_{01}$ by the factor $\eta_{\text{MF}}/2 \approx 1.18$ at the benchmark $N = 370$.

Correct interpretation of the two-channel structure

In the mesoscopic secular window:

- $\text{Re}(\rho_{PR})$: pure exponential decay at $\gamma_\phi G_{\text{loc}}$ (Eq. (45)). This is the order-parameter decoherence rate, exact within the SCS approximation.
- $\text{Im}(\rho_{PR})$ and $\rho_{PP} - \rho_{RR}$: damped oscillations at frequency ΔE with amplitude envelope decaying at $\gamma_\phi G_{\text{loc}}/2$ (Eq. (51)). This is *not* a pure exponential decay. To understand the connection to the eigenstate basis, recall from Eq. (8) that the eigenstate coherence is built exactly from these two components: $\rho_{01} = \frac{1}{2}(\rho_{PP} - \rho_{RR}) - i\text{Im}(\rho_{PR})$. Therefore, the damped oscillations of these localised variables are simply the basis-transformed view of ρ_{01} rotating at the tunnel frequency. The condition for these oscillations to be underdamped ($\Delta E \gg \gamma_\phi G_{\text{loc}}/2$) is physically equivalent to the secular condition ($2\Delta E \cdot T_2/\hbar \gg 1$). Thus, the regime where these localised variables oscillate rapidly rather than decaying exponentially is precisely the regime where the secular approximation for ρ_{01} is valid.

- These two channels are physically distinct: the real part measures order-parameter relaxation; the imaginary part measures quantum phase coherence oscillating at the tunnel frequency.

B.4 Why $\delta G \sim \mathcal{O}(N)$

The correction $\delta G = (Nm_*/2)^2 - G_{01}$ satisfies $\delta G \sim \mathcal{O}(N)$. The physical mechanism is Bogoliubov spin-wave depletion, not the zero-point variance of the energy eigenstate. Here is the correct derivation.

Key preliminary: The energy eigenstate $|E_0\rangle$ is a symmetric superposition of two non-orthogonal instanton wavepackets: $|E_0\rangle \simeq (|\tilde{P}\rangle + |\tilde{R}\rangle)/\sqrt{2}$. By parity, $\langle E_0|\hat{J}_z|E_0\rangle = 0$ exactly. Therefore the identity $\langle \hat{J}_z^2 \rangle = \langle \hat{J}_z \rangle^2 + \langle \Delta \hat{J}_z^2 \rangle$ yields $\langle E_0|\hat{J}_z^2|E_0\rangle = 0 + \langle \Delta \hat{J}_z^2 \rangle_{|E_0\rangle}$, which is positive — but this cannot explain why G_{01} is *below* the mean-field reference $(Nm_*/2)^2$.

The correct mechanism: $G_{01} \simeq J_{01}^2$ (dropping the $k \geq 2$ leakage, Section 3.4), and:

$$\delta G_{\text{Bog}} \equiv \left(\frac{Nm_*}{2}\right)^2 - J_{01}^2 \simeq Nm_*\Delta_{\text{zp}} - \Delta_{\text{zp}}^2 \sim \mathcal{O}(N),$$

where $\Delta_{\text{zp}} \sim \mathcal{O}(1)$ is the Bogoliubov zero-point depletion of the pointer-state magnetisation. The cross-term $-Nm_*\Delta_{\text{zp}} \sim \mathcal{O}(N)$ is a large *negative* correction that dominates the positive $\Delta_{\text{zp}}^2 \sim \mathcal{O}(1)$ term. Hence:

$$\delta G_{\text{Bog}} \simeq Nm_*\Delta_{\text{zp}} - \Delta_{\text{zp}}^2 \sim \mathcal{O}(N).$$

The sign is correct: subtracting a smaller value gives $\delta G_{\text{Bog}} > 0$.

Numerical verification at $N = 370$: $J_{01} = 49.51$, $Nm_*/2 = 57.77$, so $\Delta_{\text{zp}} = 8.26$. Then $Nm_*\Delta_{\text{zp}} = 2 \times 57.77 \times 8.26 = 954$ and $\Delta_{\text{zp}}^2 = 68$, giving $\delta G_{\text{Bog}} \approx 954 - 68 = 886$ vs. the direct value $(Nm_*/2)^2 - J_{01}^2 = 3337 - 2451 = 886$. ✓

The exact doublet average is $G_{01} = J_{01}^2 + (\text{average leakage}) = 2451 + 388 = 2839$, while $(Nm_*/2)^2 = 3337$, giving a true exact $\delta G_{\text{total}} = 3337 - 2839 = 498 \approx 1.35N$. Subtracting the average leakage (388) from the Bogoliubov expansion term (886) yields $886 - 388 = 498$, matching the exact finite- N result perfectly and validating the theoretical $\mathcal{O}(N)$ scaling mechanism.

Caveat. The Bogoliubov argument is the standard WKB result valid deep in the ordered phase ($\Gamma/J \ll 1$). Closer to the quantum-critical point, the depletion Δ_{zp} acquires sub-leading corrections from anharmonicity and the diverging correlation length [6]; these modify the prefactor of $\delta G/N$ but not the $\mathcal{O}(N)$ scaling.

B.5 Two sources of error: instantons vs. Bogoliubov depletion

It is important to distinguish two completely separate sources of error in the localised-rate derivation, which operate at very different scales.

Error 1 — Vacuum overlap and instanton tunnelling ($\mathcal{O}(S)$ and $\mathcal{O}(e^{-NS_{\text{inst}}})$): The eigenstate expansions (4)–(5) carry wavefunction corrections $\mathcal{O}(S)$, governed by the instanton-vacuum overlap $S = \langle \tilde{P}|\tilde{R}\rangle = (\Gamma/J)^N \approx 5.7 \times 10^{-9}$ (Section 2), which describes how closely $|E_0\rangle$ approximates $(|\tilde{P}\rangle + |\tilde{R}\rangle)/\sqrt{2}$. Separately, the energy splitting ΔE is governed by the larger dynamical scale $\mathcal{O}(e^{-NS_{\text{inst}}})$, where S_{inst} is the WKB instanton action for tunnelling through the mean-field barrier [1]. For the LMG model at

$\Gamma/J = 0.95$, $S_{\text{inst}} = 0.010787$, giving a scale $e^{-NS_{\text{inst}}} \approx 1.8 \times 10^{-2}$ at $N = 370$. Both of these non-perturbative corrections are entirely negligible at $N = 370$ and are *not* related to the difference between the exact pointer state $|P\rangle$ and $|P_{\text{SCS}}\rangle$.

Error 2 — Bogoliubov spin-wave depletion ($\mathcal{O}(N^{-1})$): The further approximation $|P\rangle \simeq |P_{\text{SCS}}\rangle$ used in the localised-rate derivation introduces a *much larger*, perturbative error. The exact pointer state $|P\rangle = (|E_0\rangle + |E_1\rangle)/\sqrt{2}$ is spin-squeezed by intra-well zero-point quantum fluctuations (Bogoliubov spin-wave depletion), reducing its mean magnetisation below $Nm_*/2$ by an $\mathcal{O}(1)$ constant: $Nm_*/2 - J_{01} \approx 6-8$ for $N = 500-2000$ (numerically verified). This shift is many orders of magnitude larger than the $\mathcal{O}(e^{-NS_{\text{inst}}})$ energy-splitting correction; the two are completely unrelated in origin. The relative error from Bogoliubov depletion is $\mathcal{O}(1)/\mathcal{O}(N) = \mathcal{O}(N^{-1})$, which dominates the instanton correction at all accessible N .

The mean-field G_{loc} overestimates the exact pointer rate by $\approx 26.2\%$ at $N = 370$ (incorporating both Bogoliubov depletion and the SCS variance approximation), highlighting the $\mathcal{O}(1)$ finite- N limitations of mean-field estimates in the mesoscopic regime.

C Diagonalisation of the Degenerate Doublet Lindbladian

This appendix provides the explicit derivation of the superoperator spectrum stated in Eq. (28) and identifies the decaying and steady-state modes of the restricted doublet.

In the degenerate doublet basis $\{|E_0\rangle, |E_1\rangle\}$, the Lindblad dissipator is given by Eq. (27):

$$\mathcal{D}[\rho]_{\text{doublet}} = \gamma_\phi J_{01}^2 (\sigma_x \rho \sigma_x - \rho). \quad (53)$$

Writing the 2×2 density matrix in this basis as:

$$\rho = \begin{pmatrix} \rho_{00} & \rho_{01} \\ \rho_{10} & \rho_{11} \end{pmatrix}, \quad (54)$$

the action of the jump operator σ_x swaps the diagonal and anti-diagonal elements:

$$\sigma_x \rho \sigma_x = \begin{pmatrix} 0 & 1 \\ 1 & 0 \end{pmatrix} \begin{pmatrix} \rho_{00} & \rho_{01} \\ \rho_{10} & \rho_{11} \end{pmatrix} \begin{pmatrix} 0 & 1 \\ 1 & 0 \end{pmatrix} = \begin{pmatrix} \rho_{11} & \rho_{10} \\ \rho_{01} & \rho_{00} \end{pmatrix}. \quad (55)$$

The Lindblad equation $\dot{\rho} = \mathcal{D}[\rho]$ therefore yields a system of four coupled differential equations:

$$\dot{\rho}_{00} = \gamma_\phi J_{01}^2 (\rho_{11} - \rho_{00}), \quad (56)$$

$$\dot{\rho}_{11} = \gamma_\phi J_{01}^2 (\rho_{00} - \rho_{11}), \quad (57)$$

$$\dot{\rho}_{01} = \gamma_\phi J_{01}^2 (\rho_{10} - \rho_{01}), \quad (58)$$

$$\dot{\rho}_{10} = \gamma_\phi J_{01}^2 (\rho_{01} - \rho_{10}). \quad (59)$$

Diagonalising this system reveals four independent modes, corresponding to the four eigenvalues of the superoperator:

1. Total population (Eigenvalue 0): Adding Eqs. (56) and (57) gives:

$$\frac{d}{dt}(\rho_{00} + \rho_{11}) = 0. \quad (60)$$

The trace $\text{tr}(\rho)$ is conserved.

2. Real coherence (Eigenvalue 0): Adding Eqs. (58) and (59) gives:

$$\frac{d}{dt}(\rho_{01} + \rho_{10}) = 2\frac{d}{dt}\text{Re}(\rho_{01}) = 0. \quad (61)$$

This confirms that $\text{Re}(\rho_{01})$ is a steady state within the restricted doublet.

3. Eigenstate population difference (Eigenvalue $-2\gamma_\phi J_{01}^2$): Subtracting Eq. (57) from Eq. (56) gives:

$$\frac{d}{dt}(\rho_{00} - \rho_{11}) = -2\gamma_\phi J_{01}^2(\rho_{00} - \rho_{11}). \quad (62)$$

4. Imaginary coherence (Eigenvalue $-2\gamma_\phi J_{01}^2$): Subtracting Eq. (59) from Eq. (58) gives:

$$\frac{d}{dt}(\rho_{01} - \rho_{10}) = 2i\frac{d}{dt}\text{Im}(\rho_{01}) = -2\gamma_\phi J_{01}^2(\rho_{01} - \rho_{10}). \quad (63)$$

Finally, to connect this to the pointer basis, we use the exact definitions $|P\rangle = (|E_0\rangle + |E_1\rangle)/\sqrt{2}$ and $|R\rangle = (|E_0\rangle - |E_1\rangle)/\sqrt{2}$. The pointer populations are:

$$\rho_{PP} = \langle P|\rho|P\rangle = \frac{1}{2}(\rho_{00} + \rho_{11} + \rho_{01} + \rho_{10}), \quad (64)$$

$$\rho_{RR} = \langle R|\rho|R\rangle = \frac{1}{2}(\rho_{00} + \rho_{11} - \rho_{01} - \rho_{10}). \quad (65)$$

The pointer population difference is therefore exactly:

$$\rho_{PP} - \rho_{RR} = \rho_{01} + \rho_{10} = 2\text{Re}(\rho_{01}). \quad (66)$$

This demonstrates that the classical memory (the population difference between the left and right wells) corresponds precisely to the second zero eigenvalue, surviving as a quasi-steady state until $\mathcal{O}(N)$ leakage to higher Dicke states eventually thermalises the system.

Note on prior literature

The localised-state rate $\gamma_\phi G_{\text{loc}} = \gamma_\phi(Nm_*)^2/2$ provides a correct estimate of the dephasing of order-parameter coherences in specific contexts.⁴ Notably, as shown in Section 3.4, $\gamma_\phi G_{\text{loc}}$ is also the *correct* rate for the decaying components of eigenstate coherence in the thermodynamic limit (when the secular approximation fails and the degenerate-doublet Lindblad is treated exactly). The present paper identifies the mesoscopic secular window ($N \approx 250$ – 430) as the regime where the eigenstate rate $\gamma_\phi G_{01} \approx \gamma_\phi G_{\text{loc}}/2$ is the physically relevant quantity for quantum protocols, where the exact pointer-state rate exceeds the eigenstate rate by a factor of $\eta_{\text{exact}} \approx 1.86$, and the mean-field estimate overestimates the eigenstate rate by a factor of $\eta_{\text{MF}} \approx 2.35$ – 2.42 .

Use of AI Assistance

During the preparation of this manuscript, the author used Claude (Anthropic) and Gemini (Google) for proofreading the \LaTeX and arithmetic verifications. All numerical simulations were independently developed and executed by the author. The author has reviewed and takes full responsibility for the final content and physical conclusions of this work.

⁴See, e.g., Ref. [8], where analogous localised-state estimates are used.

References

- [1] S. Mouslopoulos, *Classically Forbidden Signatures of Quantum Coherence in the Mesoscopic Lipkin–Meshkov–Glick Model*, arXiv:2604.18638[quant-ph] (2026).
- [2] W. H. Zurek, *Decoherence, einselection, and the quantum origins of the classical*, Rev. Mod. Phys. **75**, 715 (2003).
- [3] D. A. Lidar, I. L. Chuang, and K. B. Whaley, *Decoherence-free subspaces for quantum computation*, Phys. Rev. Lett. **81**, 2594 (1998).
- [4] S. Morrison and A. S. Parkins, *Collective spin systems in dispersive optical cavity QED: Quantum phase transitions and entanglement*, Phys. Rev. A **77**, 043810 (2008).
- [5] A. Trenkwalder, G. Spagnolli, G. Semeghini, S. Coop, M. Landini, P. Castilho, L. Pezzè, G. Modugno, M. Inguscio, A. Smerzi, and M. Fattori, *Quantum phase transitions with parity-symmetry breaking and hysteresis*, Nat. Phys. **12**, 826 (2016).
- [6] R. Botet, R. Jullien, and P. Pfeuty, *Size scaling for infinitely coordinated systems*, Phys. Rev. Lett. **49**, 478 (1982).
- [7] A. Relaño, J. M. Arias, J. Dukelsky, J. E. García-Ramos, and P. Pérez-Fernández, *Decoherence as a signature of an excited-state quantum phase transition*, Phys. Rev. A **78**, 060102(R) (2008).
- [8] M. Tegmark, *Importance of quantum decoherence in brain processes*, Phys. Rev. E **61**, 4194 (2000).
- [9] D. J. Wineland, J. J. Bollinger, W. M. Itano, F. L. Moore, and D. J. Heinzen, *Spin squeezing and reduced quantum noise in spectroscopy*, Phys. Rev. A **46**, R6797 (1992).
- [10] M. Kitagawa and M. Ueda, *Squeezed spin states*, Phys. Rev. A **47**, 5138 (1993).
- [11] L. Pezzè, A. Smerzi, M. K. Oberthaler, R. Schmied, and P. Treutlein, *Quantum metrology with nonclassical states of atomic ensembles*, Rev. Mod. Phys. **90**, 035005 (2018).
- [12] A. J. Leggett and A. Garg, *Quantum mechanics versus macroscopic realism: Is the flux there when nobody looks?*, Phys. Rev. Lett. **54**, 857 (1985).
- [13] C. Emary, N. Lambert, and F. Nori, *Leggett–Garg inequalities*, Rep. Prog. Phys. **77**, 016001 (2014).
- [14] M. Kac, G. E. Uhlenbeck, and P. C. Hemmer, *On the van der Waals Theory of the Vapor-Liquid Equilibrium. I. Discussion of a One-Dimensional Model*, J. Math. Phys. **4**, 216 (1963).
- [15] H.-P. Breuer and F. Petruccione, *The Theory of Open Quantum Systems*, Oxford University Press, Oxford (2002).
- [16] H. J. Lipkin, N. Meshkov, and A. J. Glick, *Validity of many-body approximation methods for a solvable model: (I). Exact solutions and perturbation theory*, Nucl. Phys. **62**, 188 (1965).